

Scalable Durational Event Models: Application to Physical and Digital Interactions

Cornelius Fritz^{1*}, Riccardo Rastelli^{2†}, Michael Fop^{2†}, Alberto Caimo^{2†}

¹School of Computer Science and Statistics, Trinity College Dublin

²School of Mathematics and Statistics, University College Dublin

February 5, 2026

Abstract

Durable interactions are ubiquitous in social network analysis and are increasingly observed with precise time stamps. Phone and video calls, for example, are events to which a specific duration can be assigned. We term data encoding interactions with the start and end times “durational event data”. Recent advances in data collection have enabled the observation of such data over extended periods of time and between large populations of actors. Methodologically, we propose the Durational Event Model, an extension of Relational Event Models that decouples the modeling of event incidence from event duration. Computationally, we derive a fast, memory-efficient, and exact block-coordinate ascent algorithm to facilitate large-scale inference. Theoretical complexity analysis and numerical simulations demonstrate computational superiority of this approach over state-of-the-art methods. We apply the model to physical and digital interactions among college students in Copenhagen. Our empirical findings reveal that past interactions drive physical interactions, whereas digital interactions are influenced predominantly by friendship ties and prior dyadic contact.

Keywords: Block Coordinate Algorithms, Large Event Data, Relational Event Model, MM Algorithm, Network Analysis.

*Corresponding author: fritz@tcd.ie.

†Riccardo Rastelli, Michael Fop, and Alberto Caimo contributed equally to the work. Alberto Caimo conceived the original idea of the model.

1 Introduction

Driven by rapid digitization, the availability of large-scale online networks is growing at a fast pace (Lazer et al., 2009). In contrast to traditional sociometric studies, which typically span a few hundred actors in a network, digitally measured networks encompass thousands of actors and edges and are relatively easy to collect (Wagner et al., 2021). The raw observations underlying these large networks are often automatic logs with precise timestamps of events; for instance, the time an email was sent. Complementing these digital networks, wearable sociometric badges allow continuous measurements of physical interactions (Eagle and Pentland, 2006). These data encode massive networks representing relations in contexts ranging from hospital patient transfers to instant messaging platforms.

Such large-scale networks pose distinct computational and inferential challenges. Most algorithms for estimating models for network data are based on Markov chain Monte Carlo (MCMC) algorithms (Hummel et al., 2012), scaling poorly to higher parameter dimensions and larger networks. Since a growing network warrants an increasingly complex model, this error-prone regime is expected for large networks. One way to mitigate these issues of larger networks is to base inference on an approximate likelihood (Raftery et al., 2012) or online algorithms (Corneck et al., 2025). In settings with latent variables, variational approximations are often employed, turning sampling from a posterior via MCMC into an optimization problem. For the resulting optimization problem, Minorization-Maximization (MM) algorithms were devised to obtain robust and scalable algorithms (Vu et al., 2013).

Often, one can represent these networks as sequences of events that are observed continuously in the time interval $\mathcal{T} := [0, T]$ between actors in the set $\mathcal{N} := \{1, \dots, N\}$. Relational event models (REMs, Butts, 2008) provide a framework for analyzing such events by specifying a joint stochastic process $\mathbf{N}(t) = (N_{i,j}(t))$ that counts all possible events up to time t . For each pair of actors $(i, j) \in \mathcal{D} := \{(i, j) : \{i, j\} \subseteq \mathcal{N}, i < j \text{ and } i \neq j\}$ at time $t \in \mathcal{T}$, the

counting process $N_{i,j}(t)$ is governed by a dyadic intensity, which is a function of the history up to but not including time t , denoted by the σ -algebra $\mathcal{H}_t = \sigma(\{\mathbf{N}(u) : u < t\})$:

$$\lambda_{i,j}(t \mid \mathcal{H}_t, \boldsymbol{\theta}) = g\left(\boldsymbol{\theta}^\top \mathbf{s}_{i,j}(\mathcal{H}_t)\right). \quad (1)$$

The summary statistics $\mathbf{s}_{i,j}(\mathcal{H}_t) \in \mathbb{R}^p$ for actors i and j are functions of \mathcal{H}_t . An entry of $\mathbf{s}_{i,j}(\mathcal{H}_t)$ might be the count of common partners between actors i and j until t . These statistics are weighted by the parameter $\boldsymbol{\theta} \in \mathbb{R}^p$. The function $g : \mathbb{R} \rightarrow \mathbb{R}^+$ is a non-decreasing twice differentiable function, which is commonly the identity, $g : x \mapsto x$, or exponential function $g : x \mapsto \exp(x)$, depending on the sufficient statistics affecting the dyadic intensity additively or multiplicatively. With $\mathbf{s}_{i,j}(\mathcal{H}_t) = (1, \int_0^t \exp(-(t-u)) \mathrm{d}N_{i,j}(u))^\top$, the former case encompasses Hawkes processes (Passino and Heard, 2023). In the latter case, the model corresponds to the original formulation of Butts (2008). This model class is widely used in social science (see, e.g., Kitts et al., 2017) and was extended to account for spurious events (Fritz et al., 2023) and uncover latent communities (Matias et al., 2018) to name a few. To manage the large size of event data, caching (Vu et al., 2011) and sampling-based procedures (Lerner and Lomi, 2020) were introduced.

Although time stamps are often available for durable ties, relational event modeling has so far almost exclusively focused on events without any duration. Many time-dependent interactions, such as phone or Zoom calls, naturally have a temporal duration associated with each observed event. We introduce the term ‘‘durational event’’ to describe this particular type of event. Differentiating between duration and incidence is crucial for understanding the strength and dynamics of interactions. While duration captures interaction depth and time investment, engagement and volume are reflected in frequency of occurrences, offering complementary insights. One way to model such data is to treat the duration of an event as an attached weight or mark and use a model for weighted events (Lerner et al., 2013). However, this representation disregards that the duration of an interaction is an endogenous

process, influenced by factors that arise during the interaction itself or by external factors, rather than being determined at the start of the interaction.

Stadtfeld et al. (2017) took first steps toward analyzing a related data structure by proposing a model for coordination ties. These ties are a particular case of durational events, where the creation of a link between two actors is a two-sided decision process. Still, their application focused solely on the incidence of events, disregarding their duration. Hoffman et al. (2020) introduced a model for group-based interactions, where actors can join and leave groups and Rastelli and Fop (2020) propose a stochastic block model for durational events.

Despite these initial steps, there is a gap in the literature on how to model general durational events beyond the discussed special cases. We address this limitation by introducing the Durational Event Model (DEM) as a general framework for analyzing durational events in Section 2. The DEM is related to the Separable Temporal Exponential Random Graph Model (STERGM, Krivitsky and Handcock, 2014) and Stochastic Actor-Oriented Models with gratification functions (Snijders and Van Duijn, 1997), which similarly model tie formation and dissolution. However, our framework assumes continuous observations, while the mentioned approaches model snapshots of networks at discrete times. The DEM faces the aforementioned challenges of large-scale networks, since its number of parameters grows with the number of actors and length of the observed time-frame. Thus, standard techniques, such as the Newton-Raphson method, are impractical for estimation in most applications. We develop in Section 3 a block-coordinate ascent method based on separate minorization-maximization and closed-form steps to overcome this limitation. In Section 4, we assess the performance of our algorithm in a simulation study. Next, we apply our model class to physical and digital interaction data from the Copenhagen Networks Study (Sapiezynski et al., 2019) in Section 5. Finally, we discuss possible future extensions in Section 6. Our method is implemented in the DEM package for R available at:

2 Durational Event Model

A durational event between the pair of actors $(i, j) \in \mathcal{D}$, beginning at time $t_b \in \mathcal{T}$ and ending at time $t_e \in \mathcal{T}$, with $t_b < t_e$, is represented by the four-dimensional tuple $d = (i, j, t_b, t_e)$. Henceforth, we focus on undirected durational events, although extending the methodology to directed events is straightforward. We define by $\mathcal{D}^{0 \rightarrow 1}(t) \subseteq \mathcal{D}$ the set of possible actor pairs that may experience the start of a durational event at $t \in \mathcal{T}$ (i.e., change from a “not interacting” status, denoted with 0, to an “interacting” status, denoted with 1). Similarly, $\mathcal{D}^{1 \rightarrow 0}(t) \subseteq \mathcal{D}$ is the set of possible actor pairs that may experience the end of a durational event at $t \in \mathcal{T}$. We constrain these sets such that $\mathcal{D}^{0 \rightarrow 1}(t) \cap \mathcal{D}^{1 \rightarrow 0}(t) = \emptyset$ holds, to guarantee that an interaction between a pair cannot be started and ended at the same time. Then $\mathcal{D}^{0 \rightarrow 1}(t) \cup \mathcal{D}^{1 \rightarrow 0}(t) := \mathcal{D}(t)$ denotes the set of dyads where an event can be observed at time $t \in \mathcal{T}$. To account for sparse interaction, one can define these sets to pick which dyads are governed by the specified model (Kreiß et al., 2019; Matias et al., 2018). If durational events correspond to phone calls, actors may only engage in one interaction at a time, which is represented by a constraint on these sets: observing call event (i, j, t_b, t_e) , implies that $(i, h) \notin \mathcal{D}(u)$ for $u \in [t_b, t_e]$ and $h \neq j$. We assume that these sets are known for any $t \in \mathcal{T}$.

2.1 Model Specification

To model the dynamics of durational events, we specify the DEM via two separate counting processes: the formation process, $N_{i,j}^{0 \rightarrow 1}(t)$, counting the number of times that i and j have started an interaction up to time point t ; and the dissolution process, $N_{i,j}^{1 \rightarrow 0}(t)$, counting the number of times that the actors have stopped interacting before and up to t . Together, the two stochastic processes $\mathbf{N}^{0 \rightarrow 1}(t) = (N_{i,j}^{0 \rightarrow 1}(t))$ and $\mathbf{N}^{1 \rightarrow 0}(t) = (N_{i,j}^{1 \rightarrow 0}(t))$

count the frequency with which all actor pairs transition between the states “not interacting” and “interacting” until time $t \in \mathcal{T}$. We characterize these processes by their respective instantaneous probabilities of a jump, called the incidence intensity, $\lambda_{i,j}^{0 \rightarrow 1}(t \mid \mathcal{H}_t)$, and the duration intensity, $\lambda_{i,j}^{1 \rightarrow 0}(t \mid \mathcal{H}_t)$.

The incidence and duration intensities between actors i and j in \mathcal{N} in the DEM may be influenced by their previous interactions, past interactions involving common neighbors, and ongoing interactions within the broader population. We adopt the multiplicative form with $g : x \mapsto \exp(x)$ from (1) with a self-excitation mechanism based on occurrences. This contrasts Hawkes process, which usually have an additive form with self-excitation driven by the length of time since previous events. As such, our work is more aligned with established models in the social sciences (Butts, 2008), and computationally tractable due to piecewise-constant intensities, upon which our algorithm from Section 3 relies. The intensities $\lambda_{i,j}^{0 \rightarrow 1}(t)$ and $\lambda_{i,j}^{1 \rightarrow 0}(t)$ are defined as \mathcal{H}_t -predictable functions of the observed process history:

$$\begin{aligned} \lambda_{i,j}^{0 \rightarrow 1}(t \mid \mathcal{H}_t, \boldsymbol{\theta}^{0 \rightarrow 1}) &= \exp\left(\boldsymbol{\alpha}^{0 \rightarrow 1} \mathbf{s}_{i,j}^{0 \rightarrow 1}(\mathcal{H}_t) + \beta_i^{0 \rightarrow 1} + \beta_j^{0 \rightarrow 1} + f(t, \boldsymbol{\gamma}^{0 \rightarrow 1})\right) \\ \lambda_{i,j}^{1 \rightarrow 0}(t \mid \mathcal{H}_t, \boldsymbol{\theta}^{1 \rightarrow 0}) &= \exp\left(\boldsymbol{\alpha}^{1 \rightarrow 0} \mathbf{s}_{i,j}^{1 \rightarrow 0}(\mathcal{H}_t) + \beta_i^{1 \rightarrow 0} + \beta_j^{1 \rightarrow 0} + f(t, \boldsymbol{\gamma}^{1 \rightarrow 0})\right), \end{aligned} \quad (2)$$

for $(i, j) \in \mathcal{D}^{0 \rightarrow 1}(t)$ or $\mathcal{D}^{1 \rightarrow 0}(t)$, respectively, where

- $\mathbf{s}_{i,j}^{0 \rightarrow 1}(\mathcal{H}_t) = (s_{i,j,1}^{0 \rightarrow 1}(\mathcal{H}_t), \dots, s_{i,j,P}^{0 \rightarrow 1}(\mathcal{H}_t))^\top \in \mathbb{R}^P$ are summary statistics for the pair of actors (i, j) that are functions of the history $\mathcal{H}_t = \sigma(\{\mathbf{N}^{0 \rightarrow 1}(u), \mathbf{N}^{1 \rightarrow 0}(u) : u < t\})$. These summary statistics capture dependencies between coordinates of $\mathbf{N}^{0 \rightarrow 1}(t)$ and $\mathbf{N}^{1 \rightarrow 0}(t)$ by taking into account endogenous and exogenous processes. Endogenous processes originate from events being modeled, such as the number of common partners actors i and j had up to t , while exogenous processes encompass any covariate-driven processes that, for example, capture homophily based on gender. More details on and examples of these statistics are provided in Section 2.2.
- $\boldsymbol{\alpha}^{0 \rightarrow 1} = (\alpha_1^{0 \rightarrow 1}, \dots, \alpha_P^{0 \rightarrow 1}) \in \mathbb{R}^{1 \times P}$ are parameters corresponding to $\mathbf{s}_{i,j}^{0 \rightarrow 1}(\mathcal{H}_t)$.

- $\boldsymbol{\beta}^{0 \rightarrow 1} = (\beta_1^{0 \rightarrow 1}, \dots, \beta_N^{0 \rightarrow 1})^\top \in \mathbb{R}^N$ are popularity parameters accounting for different overall activity level of each actor.
- $f : \mathcal{T} \times \mathbb{R}^Q \mapsto \mathbb{R}$ with $f(t, \boldsymbol{\gamma}^{0 \rightarrow 1}) = \sum_{q=1}^Q \gamma_q^{0 \rightarrow 1} \mathbb{I}(c_{q-1} \leq t < c_q)$ is a step-function with user-defined intervals capturing temporal variations in the data. The indicator function $\mathbb{I}(c_{q-1} \leq t < c_q)$ takes the value 1 if $c_{q-1} \leq t < c_q$ and 0 otherwise, while the parameter vector $\boldsymbol{\gamma}^{0 \rightarrow 1} = (\gamma_1^{0 \rightarrow 1}, \dots, \gamma_Q^{0 \rightarrow 1}) \in \mathbb{R}^Q$ determines the value of f within the Q segments. To ensure identifiability, we impose $\gamma_1^{0 \rightarrow 1} = 0$. Sections 5 and B.5 provide concrete examples and sensitivity analyses for specifying this step-function.

We collect all parameters in $\boldsymbol{\theta}^{0 \rightarrow 1} := (\boldsymbol{\alpha}^{0 \rightarrow 1}, \boldsymbol{\beta}^{0 \rightarrow 1}, \boldsymbol{\gamma}^{0 \rightarrow 1})$, with analog quantities defined for the duration intensity. Both intensities are piecewise constant functions, which may change at two types of time points: the baseline change points, $\mathcal{B} := \{c_1, \dots, c_Q\}$, and the time points where events occur or the observational window ends, $\mathcal{U} := \{t_1, \dots, t_M, T\}$. Here, Q is the number of time points where the baseline intensity changes and M denotes the number of observed durational events. Therefore, $N_{i,j}^{0 \rightarrow 1}(t)$ and $N_{i,j}^{1 \rightarrow 0}(t)$ with $(i, j) \in \mathcal{D}$ are Poisson processes within an interval with constant intensity. Setting $\lambda_{i,j}^{1 \rightarrow 0}(t | \mathcal{H}_t, \boldsymbol{\theta}^{1 \rightarrow 0}) = \infty$ for all pairs at all times, shows that the REM of (1) is a special case of (2).

The observed durational events define an instantaneous adjacency matrix $\mathbf{A}(t) \in \{0, 1\}^{N \times N} = (A_{i,j}(t))$, where $A_{i,j}(t) \in \{0, 1\}$ indicates the presence ($A_{i,j}(t) = 1$) or absence ($A_{i,j}(t) = 0$) of an interaction of actor pair $(i, j) \in \mathcal{D}$ at time $t \in \mathcal{T}$. Observing durational event $d = (i, j, t_b, t_e)$ implies $A_{i,j}(t) = 1$ for $t \in [t_b, t_e]$, so that the instantaneous intensity of a state change for dyad (i, j) is given by the mixture of both intensities defined in (2):

$$\lambda_{i,j}(t | \mathcal{H}_t, \boldsymbol{\theta}) = \lambda_{i,j}^{0 \rightarrow 1}(t | \mathcal{H}_t, \boldsymbol{\theta}^{0 \rightarrow 1}) (1 - A_{i,j}(t)) + \lambda_{i,j}^{1 \rightarrow 0}(t | \mathcal{H}_t, \boldsymbol{\theta}^{1 \rightarrow 0}) A_{i,j}(t). \quad (3)$$

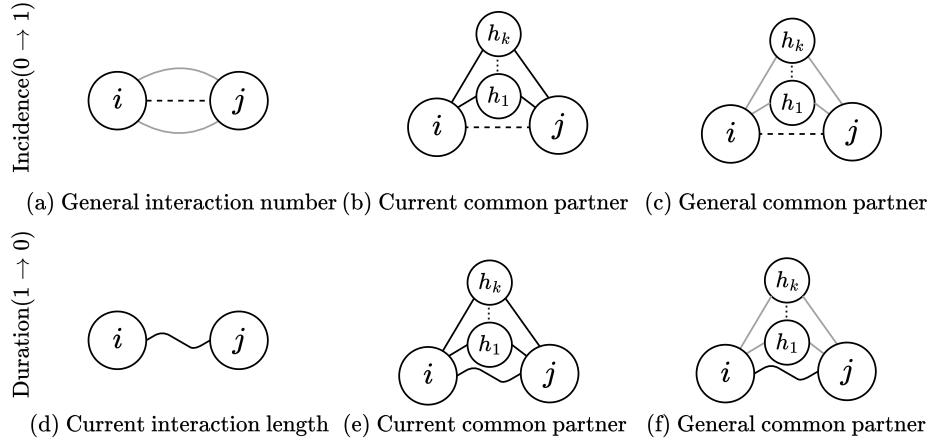


Figure 1: Graphs illustrating the proposed summary statistics. Dashed lines (--) refer to transitions from $0 \rightarrow 1$, while the wiggly line (\sim) relates to $1 \rightarrow 0$. Other observed interactions are drawn as solid lines, in black if they are currently interacting actors (—) and gray if the event occurred sometime in the past (—).

2.2 Summary Statistics

The statistics $\mathbf{s}_{i,j}^{0 \rightarrow 1}(\mathcal{H}_t)$ and $\mathbf{s}_{i,j}^{1 \rightarrow 0}(\mathcal{H}_t)$ characterize the influence of past interactions on the likelihood of future events. Careful consideration is necessary regarding how this influence is specified. Aalen and Gjessing (2007) note that a valid counting process must have an intensity function that remains finite at all times to prevent an explosion where the intensity diverges. The Feller criterion (Aalen and Gjessing, 2007, Sect. 3.2.2) guarantees non-explosion if the intensity function satisfies a linear growth bound. Applying the transformation $x \mapsto \log(x + 1)$ to past event counts in the summary statistics, ensures that the intensities in (2) satisfy this condition.

With two further exceptions, the summary statistics can then be defined similarly to their counterparts in REMs (Butts, 2008). First, we assume that the incidence and duration models rely on distinct sets of statistics. Below, we introduce statistics which can be incorporated into either $\mathbf{s}_{i,j}^{0 \rightarrow 1}(\mathcal{H}_t)$, $\mathbf{s}_{i,j}^{1 \rightarrow 0}(\mathcal{H}_t)$, or both. Second, the statistics can leverage

additional information from durational events, such as which actors are currently interacting. Let $u_{i,j}(t)$ be a binary indicator whether actors i and j have started an interaction that is still ongoing at time t , and let $v_{i,j}(t)$ indicate whether they have interacted before time t . The elapsed time since actors i and j started their interaction to time t is $\Delta_{i,j}(t)$. Given these quantities, we provide a list of exemplary summary statistics used in simulations and the application, accompanied by illustrations in Figure 1:

- $s_{i,j,CCP}(\mathcal{H}_t) = \log\left(\sum_{h \notin \{i,j\}} u_{i,h}(t) u_{h,j}(t) + 1\right)$: statistic representing the number of currently active partners shared by i and j at time t ;
- $s_{i,j,GCP}(\mathcal{H}_t) = \log\left(\sum_{h \notin \{i,j\}} v_{i,h}(t) v_{h,j}(t) + 1\right)$: statistic representing the number of general common partners of i and j up to time t ;
- $s_{i,j,NI}(\mathcal{H}_t) = \log(N_{i,j}(t) + 1)$: statistic representing the cumulative sum of interactions between i and j up to time t ;
- $s_{i,j,IL}^{1 \rightarrow 0}(\mathcal{H}_t) = \log(\Delta_{i,j}(t^*) + 1)$: interaction length statistic representing the duration of the current interaction between actors i and j until time t^* ;
- $s_{i,j,z}(\mathcal{H}_t) = z_{i,j}$: dyadic covariate effect, where, e.g., $z_{i,j} = |x_{i,1} - x_{j,1}|$ or $z_{i,j} = \mathbb{I}(x_{i,2} = x_{j,2})$ depending on whether the effect is based on a categorical, $\mathbf{x}_1 = (x_{1,1}, \dots, x_{N,1})$, or continuous, $\mathbf{x}_2 = (x_{1,2}, \dots, x_{N,2})$, exogenous covariate.

Parallels between the DEM and proportional hazard model facilitate interpreting the estimated coefficients. Consider the incidence intensities of two durational events $d_1 = (i, j, t, t_e)$ and $d_2 = (h, k, t, t_e)$. Assuming that all summary statistics are identical with the exception that the p th entry of the summary statistics for d_1 is one unit higher than for d_2 (i.e., $s_{i,j,p}(\mathcal{H}_t) = s_{h,k,p}(\mathcal{H}_t) + 1$), the relationship between their intensities to start an interaction at time t is:

$$\lambda_{i,j}^{0 \rightarrow 1}(t|\mathcal{H}_t, \boldsymbol{\theta}^{0 \rightarrow 1}) = \exp(\alpha_p^{0 \rightarrow 1}) \lambda_{h,k}^{0 \rightarrow 1}(t|\mathcal{H}_t, \boldsymbol{\theta}^{0 \rightarrow 1}). \quad (4)$$

Put differently, with $\alpha_p^{0 \rightarrow 1} > 0$, observing d_1 is $\exp(\alpha_p^{0 \rightarrow 1})$ times more likely than d_2 .

We log-transform statistics involving counts of past events, such as the number of current common partners between actors i and j until time t . Similar to geometrically weighted statistics in the context of ERGMs (Hunter, 2007), this transformation formalizes the intuition that the initial change in a statistic has the greatest impact with subsequent changes having diminishing returns. A change from l to $l + 1$ on the original scale of a $\log(\cdot + 1)$ -transformed statistic affects the intensity by the multiplicative factor $((l + 2)/(l + 1))^{\alpha_p^{0 \rightarrow 1}}$. Setting $l = 0$, the quantity $2^{\alpha_p^{0 \rightarrow 1}}$ represents the multiplicative effect of the first unit increase of a statistic on its original scale and is therefore a valuable tool to interpret the model. For $s_{i,j,p}^{0 \rightarrow 1}(\mathcal{H}_t) = s_{i,j,GCP}^{0 \rightarrow 1}(\mathcal{H}_t)$, the first common partner has the multiplicative effect $2^{\alpha_p^{0 \rightarrow 1}}$, while the 20th common partner has the multiplicative effect $(21/20)^{\alpha_p^{0 \rightarrow 1}} = 1.05^{\alpha_p^{0 \rightarrow 1}}$ on the incidence intensity between actors i and j . This illustrates how dependence between counting processes is induced via a shared history \mathcal{H}_t : assuming that actors i and j are in an interaction at time t and $N_{j,h}^{0 \rightarrow 1}(t) > 0$, a jump in $N_{i,h}^{0 \rightarrow 1}(t)$ affects the intensity of a jump in $N_{i,j}^{1 \rightarrow 0}(t)$ if the statistic $s_{i,j,GCP}^{1 \rightarrow 0}(\mathcal{H}_t)$ is included in the model.

3 Scalable Block-Coordinate Ascent Algorithm

Given the paths of $N_{i,j}^{0 \rightarrow 1}(t)$ and $N_{i,j}^{1 \rightarrow 0}(t)$ with $(i, j) \in \mathcal{D}$ and $t \in \mathcal{T}$, we propose a scalable method to estimate $\boldsymbol{\theta}^{0 \rightarrow 1}$ and $\boldsymbol{\theta}^{1 \rightarrow 0}$ maximizing the log-likelihood

$$\ell^*(\boldsymbol{\theta}^{0 \rightarrow 1}, \boldsymbol{\theta}^{1 \rightarrow 0}) \propto \ell^{0 \rightarrow 1}(\boldsymbol{\theta}^{0 \rightarrow 1}) + \ell^{1 \rightarrow 0}(\boldsymbol{\theta}^{1 \rightarrow 0}), \quad (5)$$

which is separable with respect to $\boldsymbol{\theta}^{0 \rightarrow 1}$ and $\boldsymbol{\theta}^{1 \rightarrow 0}$. This separability stems from the definition of the DEM as a multivariate counting process where the formation and dissolution intensities are conditionally independent given the sufficient statistics, time, and current interaction status of dyads. Thus, we independently estimate the incidence and duration model using

the same procedure. Let $\boldsymbol{\theta} = (\boldsymbol{\alpha}, \boldsymbol{\beta}, \boldsymbol{\gamma})$, $\mathcal{D}(t)$, $\ell(\boldsymbol{\theta})$, and $\mathbf{s}_{i,j}(\mathcal{H}_t)$ correspond to either $\boldsymbol{\theta}^{0 \rightarrow 1}$ or $\boldsymbol{\theta}^{1 \rightarrow 0}$, $\ell^{0 \rightarrow 1}(\boldsymbol{\theta}^{0 \rightarrow 1})$ or $\ell^{1 \rightarrow 0}(\boldsymbol{\theta}^{1 \rightarrow 0})$, $\mathcal{D}^{0 \rightarrow 1}(t)$ or $\mathcal{D}^{1 \rightarrow 0}(t)$, and $\mathbf{s}_{i,j}^{0 \rightarrow 1}(\mathcal{H}_t)$ or $\mathbf{s}_{i,j}^{1 \rightarrow 0}(\mathcal{H}_t)$, depending on estimating $\boldsymbol{\theta}^{0 \rightarrow 1}$ or $\boldsymbol{\theta}^{1 \rightarrow 0}$. The log-likelihood of each sub-model in (5) is then:

$$\ell(\boldsymbol{\theta}) = \sum_{t \in \mathcal{B} \cup \mathcal{U}} \sum_{(i,j) \in \mathcal{D}(t)} y_{i,j,t} \log((t - t^*) \lambda_{i,j}(t | \mathcal{H}_t, \boldsymbol{\theta})) - (t - t^*) \lambda_{i,j}(t | \mathcal{H}_t, \boldsymbol{\theta}), \quad (6)$$

where $y_{i,j,t} \in \{0, 1\}$ indicates whether a formation or dissolution event occurred between actors i and j in the time interval from t^* to t . Here, t^* denotes the most recent time point before t within the specific ordered set over which the summation index t iterates. For the chronologically first time point in this set, we set $t^* = 0$. The estimate of $\boldsymbol{\theta}$ in the k th iteration of $\boldsymbol{\theta}$ is denoted by $\boldsymbol{\theta}^{(k)}$.

The Newton-Raphson method is the state-of-the-art technique for estimating $\boldsymbol{\theta}$ in REMs (Butts, 2008; Stadtfeld et al., 2017), updating $\boldsymbol{\theta}^{(k+1)}$ by the following rule:

$$\boldsymbol{\theta}^{(k+1)} = \boldsymbol{\theta}^{(k)} - \boldsymbol{\Sigma}(\boldsymbol{\theta}^{(k)})^{-1} \mathbf{g}(\boldsymbol{\theta}^{(k)}), \quad (7)$$

where $\mathbf{g}(\boldsymbol{\theta}^{(k+1)}) := \nabla_{\boldsymbol{\theta}} \ell(\boldsymbol{\theta}) \Big|_{\boldsymbol{\theta}=\boldsymbol{\theta}^{(k+1)}}$ and $\boldsymbol{\Sigma}(\boldsymbol{\theta}^{(k+1)}) := \nabla_{\boldsymbol{\theta}}^2 \ell(\boldsymbol{\theta}) \Big|_{\boldsymbol{\theta}=\boldsymbol{\theta}^{(k+1)}}$ denote the gradient and Hessian of (6) evaluated at $\boldsymbol{\theta}^{(k+1)} \in \mathbb{R}^{P+N+Q}$, respectively. The per-iteration computational complexity for this algorithm is $O(N^2(N+Q)^2(Q+M))$, assuming $N \geq 2$ and P is fixed (i.e., $P = O(1)$). In most real-world settings, data is available across many actors (large N) and over an extensive time interval (large Q), making the estimation $\boldsymbol{\theta}$ via (7) impractical. To bypass this computational burden, we devise a block-coordinate ascent algorithm:

Step 1: Set $\boldsymbol{\alpha}^{(k+1)}$ such that $\ell(\boldsymbol{\alpha}^{(k+1)}, \boldsymbol{\beta}^{(k)}, \boldsymbol{\gamma}^{(k)}) \geq \ell(\boldsymbol{\alpha}^{(k)}, \boldsymbol{\beta}^{(k)}, \boldsymbol{\gamma}^{(k)})$ by a Newton-Raphson update.

Step 2: Set $\boldsymbol{\beta}^{(k+1)}$ such that $\ell(\boldsymbol{\alpha}^{(k+1)}, \boldsymbol{\beta}^{(k+1)}, \boldsymbol{\gamma}^{(k)}) \geq \ell(\boldsymbol{\alpha}^{(k+1)}, \boldsymbol{\beta}^{(k)}, \boldsymbol{\gamma}^{(k)})$ by a Minorization-Maximization update (12).

Step 3: Set $\boldsymbol{\gamma}^{(k+1)}$ such that $\ell(\boldsymbol{\alpha}^{(k+1)}, \boldsymbol{\beta}^{(k+1)}, \boldsymbol{\gamma}^{(k+1)}) \geq \ell(\boldsymbol{\alpha}^{(k+1)}, \boldsymbol{\beta}^{(k+1)}, \boldsymbol{\gamma}^{(k)})$ by a closed form update (14).

The blockwise algorithm offers several computational advantages: first, the complexity per iteration compared to the Newton-Raphson update in (7) is reduced from $O((N + Q)^2 N^2 (Q + M))$ to $O((N^2 + M) Q + MN)$. This improvement is achieved by restricting matrix inversions to the first step, leveraging the low dimensionality of $\boldsymbol{\alpha}$ to ensure scalability with respect to N and Q . In that step, we also employ caching algorithms. Second, there is no need to store large matrices at any step, reducing memory usage. Third, we obtain global convergence to the maximum likelihood estimator $\boldsymbol{\theta}^*$, i.e., $\boldsymbol{\theta}^{(k)} \rightarrow \boldsymbol{\theta}^*$ with $k \rightarrow \infty$ for any starting value $\boldsymbol{\theta}^{(0)}$. This property holds since the likelihood function (6) can be decomposed into sums of likelihoods of Poisson-distributed random variables (Fritz et al., 2023), making $\ell(\boldsymbol{\theta})$ a strictly concave function. We therefore seed our algorithm by setting $\boldsymbol{\theta}^{(0)} = \mathbf{0}_{P+N+Q}$, being a $(P + N + Q)$ -dimensional vector filled with zeros. Fourth, contrasting the Newton-Raphson method, our algorithm enjoys the ascent property, $\ell(\boldsymbol{\alpha}^{(k+1)}, \boldsymbol{\beta}^{(k+1)}, \boldsymbol{\gamma}^{(k+1)}) \geq \ell(\boldsymbol{\alpha}^{(k)}, \boldsymbol{\beta}^{(k)}, \boldsymbol{\gamma}^{(k)})$, making the algorithm robust and reliable. Fifth, our algorithm naturally extends to standard REMs. Convergence is declared once both $\|\boldsymbol{\theta}^{(k+1)} - \boldsymbol{\theta}^{(k)}\|_2$ and $|(\ell(\boldsymbol{\theta}^{(k+1)}) - \ell(\boldsymbol{\theta}^{(k)})) / \ell(\boldsymbol{\theta}^{(k)})|$ are below a given threshold, typically set at 10^{-3} . We next describe the algorithm in detail.

Step 1: Update of $\boldsymbol{\alpha}$. Similar to (7), we employ Newton-Raphson updates for $\boldsymbol{\alpha}$ with:

$$\begin{aligned} \nabla_{\boldsymbol{\alpha}} \ell(\boldsymbol{\alpha}, \boldsymbol{\beta}^{(k)}, \boldsymbol{\gamma}^{(k)}) \Big|_{\boldsymbol{\alpha}=\boldsymbol{\alpha}^{(k)}} &= \sum_{(i,j) \in \mathcal{D}} \sum_{t \in \mathcal{U}} \mathbf{s}_{i,j}(\mathcal{H}_t) \left(y_{i,j,t} - \int_{t^*}^t \lambda_{i,j}(u \mid \mathcal{H}_u, \boldsymbol{\theta}^{(k)}) du \right) \\ \nabla_{\boldsymbol{\alpha}}^2 \ell(\boldsymbol{\alpha}, \boldsymbol{\beta}^{(k)}, \boldsymbol{\gamma}^{(k)}) \Big|_{\boldsymbol{\alpha}=\boldsymbol{\alpha}^{(k)}} &= - \sum_{(i,j) \in \mathcal{D}} \sum_{t \in \mathcal{U}} \mathbf{s}_{i,j}(\mathcal{H}_t)^{\otimes 2} \left(\int_{t^*}^t \lambda_{i,j}(u \mid \mathcal{H}_u, \boldsymbol{\theta}^{(k)}) du \right), \end{aligned} \quad (8)$$

where $\mathbf{s}_{i,j}(\mathcal{H}_t)^{\otimes 2} := \mathbf{s}_{i,j}(\mathcal{H}_t) \mathbf{s}_{i,j}(\mathcal{H}_t)^\top$. Because the intensity function is piecewise-constant, the integral $\int_{t^*}^t \lambda_{i,j}(u \mid \mathcal{H}_u, \boldsymbol{\theta}) du$ admits an exact computation. Inspired by caching algorithms introduced in Vu et al. (2011), we only update the summary statistics corresponding to pairs affected by d after observing the event d at time t . Since all summary statistics in Section 2.2 are defined locally, we assume that each interaction solely affects a subset of

pairs scaling with $O(N)$. Under $P = O(1)$, the complexity of this step is then $O(N^2 + MN)$, eliminating the dependence on the number of change points of the baseline intensity in contrast to (6)

Step 2: Update of β . A Newton-Raphson update for β is computationally infeasible due to the dimension of β being N . To avoid this bottleneck, we derive a Minorization-Maximization (MM) algorithm (Lange et al., 2000). Within this algorithm, we define a surrogate function with a closed-form solution whose maximizer guarantees $\ell(\alpha^{(k+1)}, \beta^{(k+1)}, \gamma^{(k)}) \geq \ell(\alpha^{(k+1)}, \beta^{(k)}, \gamma^{(k)})$. To derive this function, we first reformulate $\ell(\alpha^{(k+1)}, \beta, \gamma^{(k)})$, being a function of β with fixed $\alpha = \alpha^{(k+1)}$ and $\gamma = \gamma^{(k)}$:

$$\ell(\alpha^{(k+1)}, \beta, \gamma^{(k)}) \propto \sum_{(i,j) \in \mathcal{D}} (\log p_i + \log p_j) \left(\sum_{t \in \mathcal{U}} y_{i,j,t} \right) - p_i p_j \left(\sum_{t \in \mathcal{U}} p_{i,j,t} \right), \quad (9)$$

where

$$p_{i,j,t} := \left(\int_{t^*}^t \exp(f(u, \gamma^{(k)})) du \right) \exp(\alpha^{(k+1)} \mathbf{s}_{i,j}(\mathcal{H}_t))$$

and $p_i := \exp(\beta_i)$ for $t \in \mathcal{U}$ and $(i, j) \in \mathcal{D}$. By the AM–GM inequality, we get

$$p_i p_j \leq \frac{p_j^{(k)}}{2 p_i^{(k)}} p_i^2 + \frac{p_i^{(k)}}{2 p_j^{(k)}} p_j^2, \quad (10)$$

allowing us define a surrogate function $m(\beta \mid \alpha^{(k+1)}, \beta^{(k)}, \gamma^{(k)})$:

$$\begin{aligned} \ell(\alpha^{(k+1)}, \beta, \gamma^{(k)}) &\geq \sum_{(i,j) \in \mathcal{D}} (\log p_i + \log p_j) \left(\sum_{t \in \mathcal{U}} y_{i,j,t} \right) \\ &\quad - \left(\frac{p_j^{(k)}}{2 p_i^{(k)}} p_i^2 + \frac{p_i^{(k)}}{2 p_j^{(k)}} p_j^2 \right) \left(\sum_{t \in \mathcal{U}} p_{i,j,t} \right) \\ &=: m(\beta \mid \alpha^{(k+1)}, \beta^{(k)}, \gamma^{(k)}). \end{aligned}$$

Since equality holds in (10) with $p = p^{(k)}$ and $p^{(k)} := \exp(\beta^{(k)})$, two properties hold:

$$\begin{aligned} m(\beta \mid \alpha^{(k+1)}, \beta^{(k)}, \gamma^{(k)}) &\leq \ell(\alpha^{(k+1)}, \beta, \gamma^{(k)}) \quad \text{for all } \beta \in \mathbb{R}^P \\ m(\beta^{(k)} \mid \alpha^{(k+1)}, \beta^{(k)}, \gamma^{(k)}) &= \ell(\alpha^{(k+1)}, \beta^{(k)}, \gamma^{(k)}), \end{aligned} \quad (11)$$

making $m(\boldsymbol{\beta} \mid \boldsymbol{\alpha}^{(k+1)}, \boldsymbol{\beta}^{(k)}, \boldsymbol{\gamma}^{(k)})$ a minorizer of $\ell(\boldsymbol{\alpha}^{(k+1)}, \boldsymbol{\beta}, \boldsymbol{\gamma}^{(k)})$ in $\boldsymbol{\beta}^{(k)}$. Applying these inequalities shows that setting $\boldsymbol{\beta}^{(k+1)}$ to the value maximizing $m(\boldsymbol{\beta} \mid \boldsymbol{\alpha}^{(k+1)}, \boldsymbol{\beta}^{(k)}, \boldsymbol{\gamma}^{(k)})$ with respect to $\boldsymbol{\beta}$, guarantees $\ell(\boldsymbol{\alpha}^{(k+1)}, \boldsymbol{\beta}^{(k+1)}, \boldsymbol{\gamma}^{(k)}) \geq \ell(\boldsymbol{\alpha}^{(k+1)}, \boldsymbol{\beta}^{(k)}, \boldsymbol{\gamma}^{(k)})$. In contrast to $\ell(\boldsymbol{\alpha}^{(k+1)}, \boldsymbol{\beta}, \boldsymbol{\gamma}^{(k)})$, $m(\boldsymbol{\beta} \mid \boldsymbol{\alpha}^{(k+1)}, \boldsymbol{\beta}^{(k)}, \boldsymbol{\gamma}^{(k)})$ has a closed form solution for β for $i \in \mathcal{N}$:

$$\beta_i^{(k+1)} = \log \left(\sqrt{\frac{\sum_{j \neq i} \sum_{t \in \mathcal{U}} y_{i,j,t}}{p_i^{(k)} \sum_{j \neq i} \sum_{t \in \mathcal{U}} p_{i,j,t} p_j^{(k+1)}}}} \right). \quad (12)$$

These cyclical updates for $i = 1, \dots, N$ have the algorithmic complexity $O(N(N+M))$.

Step 3: Update of $\boldsymbol{\gamma}$. With $q_{i,j,t} := \int_{t^*}^t \exp(\boldsymbol{\alpha}^{(k+1)} \mathbf{s}_{i,j}(\mathcal{H}_u) + \beta_i + \beta_j) du$ and $q_t := \exp(f(t, \boldsymbol{\gamma}))$ for $t \in \mathcal{D}$ and $(i, j) \in \mathcal{D}$, we can sort the summands of $\ell(\boldsymbol{\alpha}^{(k+1)}, \boldsymbol{\beta}^{(k+1)}, \boldsymbol{\gamma})$ according to the intervals defined through the timepoints where the baseline intensity changes, $0 = c_0 < c_1 < \dots < c_Q$:

$$\ell(\boldsymbol{\alpha}^{(k+1)}, \boldsymbol{\beta}^{(k+1)}, \boldsymbol{\gamma}) \propto \sum_{(i,j) \in \mathcal{D}} \sum_{q=1}^Q \sum_{c_{q-1} \leq t < c_q} y_{i,j,t} \log q_t - q_t q_{i,j,t}. \quad (13)$$

This function is separable with respect to all coordinates of $\boldsymbol{\gamma}$ with a closed-form solution:

$$\gamma_q^{(k+1)} = \log \left(\frac{\sum_{(i,j) \in \mathcal{D}} \sum_{c_{q-1} \leq t < c_q} y_{i,j,t}}{\sum_{(i,j) \in \mathcal{D}} \sum_{c_{q-1} \leq t < c_q} q_{i,j,t}} \right). \quad (14)$$

Employing update (14) for $q = 2, \dots, Q$ has the algorithmic complexity of $O(Q(N^2 + M))$.

Uncertainty Quantification. Under suitable regularity conditions, inference is possible in our model for growing Q and N based on the inverse of $\Sigma(\hat{\boldsymbol{\theta}})$, where $\hat{\boldsymbol{\theta}}$ are the converged parameter estimates (Portnoy, 1988). Most importantly, $N^2/M \rightarrow 0$ needs to hold with $M \rightarrow \infty$ provided $Q = O(\sqrt{M})$ so that information accumulates sufficiently fast relative to the model dimension. For regimes where Q grows faster, the combination of Portnoy (1988) with profile likelihood theory (Murphy and van der Vaart, 2000) and the Simulation Study 5 in Section A.3.3 suggest that the normal approximation for $\hat{\boldsymbol{\alpha}}$ still holds. In most

applications, interest mainly lies in quantifying the uncertainty of $\hat{\boldsymbol{\alpha}}$. Therefore, we consider $\boldsymbol{\beta}$ and $\boldsymbol{\gamma}$ to be nuisance parameters and only evaluate the top left block of the inverse Hessian, $\boldsymbol{\Sigma}(\hat{\boldsymbol{\theta}})^{-1}$, which we denote by $\boldsymbol{\Lambda}(\hat{\boldsymbol{\theta}})$:

$$\boldsymbol{\Lambda}(\hat{\boldsymbol{\theta}}) = \left(\boldsymbol{\Sigma}_{\hat{\boldsymbol{\alpha}}, \hat{\boldsymbol{\alpha}}} - \mathbf{X}_{\hat{\boldsymbol{\alpha}}, \hat{\boldsymbol{\beta}}, \hat{\boldsymbol{\gamma}}} \mathbf{Y}_{\hat{\boldsymbol{\beta}}, \hat{\boldsymbol{\gamma}}}^{-1} \mathbf{X}_{\hat{\boldsymbol{\alpha}}, \hat{\boldsymbol{\beta}}, \hat{\boldsymbol{\gamma}}}^\top \right)^{-1}, \quad (15)$$

with

$$\mathbf{X}_{\hat{\boldsymbol{\alpha}}, \hat{\boldsymbol{\beta}}, \hat{\boldsymbol{\gamma}}} = \left(\boldsymbol{\Sigma}_{\hat{\boldsymbol{\alpha}}, \hat{\boldsymbol{\beta}}} \quad \boldsymbol{\Sigma}_{\hat{\boldsymbol{\alpha}}, \hat{\boldsymbol{\gamma}}} \right) \text{ and } \mathbf{Y}_{\hat{\boldsymbol{\beta}}, \hat{\boldsymbol{\gamma}}} = \begin{pmatrix} \boldsymbol{\Sigma}_{\hat{\boldsymbol{\beta}}, \hat{\boldsymbol{\beta}}} & \boldsymbol{\Sigma}_{\hat{\boldsymbol{\beta}}, \hat{\boldsymbol{\gamma}}} \\ \boldsymbol{\Sigma}_{\hat{\boldsymbol{\beta}}, \hat{\boldsymbol{\gamma}}}^\top & \boldsymbol{\Sigma}_{\hat{\boldsymbol{\gamma}}, \hat{\boldsymbol{\gamma}}} \end{pmatrix},$$

where, e.g., matrix $\boldsymbol{\Sigma}_{\hat{\boldsymbol{\alpha}}, \hat{\boldsymbol{\beta}}}$ is the sub-block of $\boldsymbol{\Sigma}$ associated with $\hat{\boldsymbol{\alpha}}$ and $\hat{\boldsymbol{\beta}}$.

4 Simulation Study

We evaluate our estimator’s performance across three simulation studies targeting parameter recovery, uncertainty quantification, and computational improvement. The experimental design involves $S = 1,000$ simulated datasets for several actor population sizes N with covariates: one continuous covariate, $\mathbf{x} = (x_1, \dots, x_N)$ with $X_i \stackrel{\text{i.i.d.}}{\sim} \mathcal{N}(0, 1)$, and one discrete covariate, $\mathbf{y} = (y_1, \dots, y_N)$ with $Y_i \stackrel{\text{i.i.d.}}{\sim} \text{Categorical}(1/3, 1/3, 1/3)$, is available. These covariates inform the summary statistics vectors $\mathbf{s}_{i,j}^{0 \rightarrow 1} = (s_{i,j,CCP}, s_{i,j,\mathbf{x}}, s_{i,j,\mathbf{y}})^\top$ and $\mathbf{s}_{i,j}^{1 \rightarrow 0} = (s_{i,j,NI}, s_{i,j,\mathbf{x}}, s_{i,j,\mathbf{y}})^\top$, with their dependence on the history \mathcal{H}_t suppressed for notational clarity. The corresponding true parameter vectors are fixed at $\boldsymbol{\alpha}^{0 \rightarrow 1} = (-1/2, 1, 1/2)$ and $\boldsymbol{\alpha}^{1 \rightarrow 0} = (1/2, 1/2, 1/2)$, while the popularity parameters $\boldsymbol{\beta}$ are Gaussian-distributed, $\boldsymbol{\beta}^{0 \rightarrow 1}$ with $\beta_i^{0 \rightarrow 1} \stackrel{\text{i.i.d.}}{\sim} \mathcal{N}(-6 - 1/10 \log(N), 1)$ and $\boldsymbol{\beta}^{1 \rightarrow 0}$ with $\beta_i^{1 \rightarrow 0} \stackrel{\text{i.i.d.}}{\sim} \mathcal{N}(8/5 - 1/10 \log(N), 1)$, decreasing proportional to $-\log(N)$ to induce sparsity. We specify a baseline by $\boldsymbol{\gamma} = \boldsymbol{\gamma}^{0 \rightarrow 1} = \boldsymbol{\gamma}^{1 \rightarrow 0}$ which decays linearly from 0 to -0.1 over $\mathcal{T} = [0, 10,000]$. Section A provides details on the simulation algorithm, evaluation measures, and further results.

Table 1: Simulation Study 1: For each effect, we report the Bias ($\hat{\alpha} - \alpha^*$), RMSE (Root-Mean-Squared Error), and CP (Coverage Probability). The dependence of the sufficient statistics on the history \mathcal{H}_t suppressed for notational clarity.

Incidence ($\alpha^{0 \rightarrow 1}$)				Duration ($\alpha^{1 \rightarrow 0}$)			
Statistic	Bias	RMSE	CP	Statistic	Bias	RMSE	CP
$s_{i,j,CCP}$	-.010	.074	.951	$s_{i,j,NI}$.000	.010	.945
$s_{i,j,x}$	-.002	.010	.944	$s_{i,j,x}$.002	.011	.939
$s_{i,j,y}$	-.001	.010	.957	$s_{i,j,y}$.001	.011	.944

Simulation Study 1: Parameter Estimation. In the first simulation study, we assess how accurately our novel algorithm recovers the correct model for $N = 500$ actors. Table 1 demonstrates that α is estimated with high accuracy. The empirical coverage probability matches the nominal 0.95 level, indicating reliable uncertainty quantification. For the current common partner statistic, we note a higher RMSE compared to the other statistics, which may be due to the statistic using less data by only relying on the current status of the network rather than its entire history. Section A.3.1 supplements results on model selection using the Akaike Information Criterion and the normality of estimators.

Simulation Study 2: Estimation Error under Increasing Actors. We rely on an analogous setup as in Simulation Study 1, with the only difference being that the number of actor varies from 50 to 1,000. We assess the estimation error of all parameters.

For both sub-models, Figure 2 (a) shows that the RMSE of all estimated parameters decreases as the number of actors N increases. The baseline intensity and summary statistics coefficients exhibit lower estimation error than the popularity parameters, whose dimensionality grows with N . This behavior is expected due to the increasing dimension of the popularity effects. These results provide empirical evidence for the consistency of our

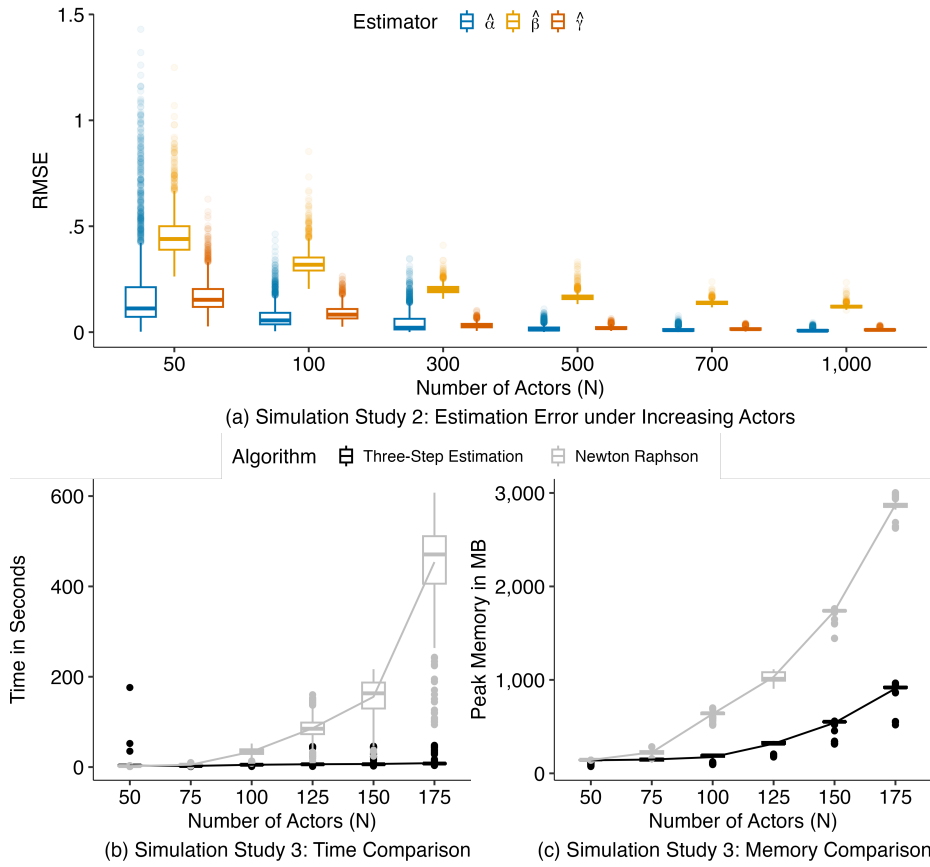


Figure 2: Simulation Study 2: (a) RMSE of $\hat{\alpha}$ (blue), $\hat{\beta}$ (yellow), and $\hat{\gamma}$ (orange) pooled over incidence and duration model. Simulation Study 3: Comparison of computational time (b) and memory needed for estimation (c) for different number of actors of our proposed three-step estimator and the state-of-the-art Newton-Raphson method.

estimators in regimes where the number of parameters is a function of the number of actors.

Simulation Study 3: Computational Improvement. Finally, we compare the computational efficiency of our novel algorithm (Section 3) to the Newton-Raphson approach. We measure computational speed by the execution time (in seconds) for estimating the model on a single dataset. Memory allocation is assessed by each algorithm’s peak random access memory usage, to reflect the largest dataset a system can handle.

Figure 2 (b) and (c) visualizes the execution time and memory usage for both algorithms

under increasing number of actors. The largest dataset we consider has only up to 175 nodes, beyond which the Newton-Raphson algorithm becomes impractical. The results provide empirical evidence that our block-coordinate ascent algorithm improves upon state-of-the-art methods by several orders of magnitude. From Figure 2 (c), it is evident that our proposed algorithm scales more efficiently than the Newton-Raphson method. Additionally, our approach exhibits lower variability in computing time and memory usage. Both findings align with the theoretical complexity reduction derived in Section 3.

5 Application to Physical and Digital Interactions

We demonstrate the DEM in an application to the Copenhagen Networks Study (Sapiezynski et al., 2019). The study, conducted between 2012 and 2013, tracked 682 first-year students at the Technical University of Denmark over approximately 28 days. This data includes various forms of interactions, such as co-location (measured via Bluetooth), social media interactions (friendships on Facebook), and other communication channels (phone calls and text messages). The available data allows comparing the evolution of physical and digital interactions between the same actors over time. Thereby, we can identify how individuals prioritize different relationships and the circumstances under which they rely on digital or face-to-face interactions (Stopczynski et al., 2014). We study digital communication through call data, while co-location events act as a proxy for physical activities. By distinguishing when interactions begin and end, we can (i) fully utilize the available data and (ii) assess whether similar factors drive both the incidence and duration of events.

Several studies have used data from the Copenhagen Networks Study for descriptive analyses. Sekara et al. (2016) demonstrate with it how interaction data with fine-grained temporal resolution can be used to examine group formation. Building on the foundational work of Granovetter (1973), Ureña-Carrion et al. (2020) investigate the strength of interactions

with the data. However, to our knowledge, no probabilistic models, such as REMs, have been applied to this dataset.

Physical interactions are quantified by co-location events, measured via Bluetooth communication between mobile devices. Bluetooth scans run every five minutes determine when people are close to one another. We define a co-location event as the presence of two individuals in at least two consecutive scans. Therefore, a physical interaction event (i, j, t_b, t_e) indicates that student i was in the same place as student j from time t_b to t_e .

Call data represent digital communication, where an event (i, j, t_b, t_e) encodes a call between student i and student j between the time points t_b and t_e . The sets $\mathcal{D}^{0 \rightarrow 1}(t)$ and $\mathcal{D}^{1 \rightarrow 0}(t)$ for $t \in \mathcal{T}$ are defined so that no student can be active in simultaneous calls (see Section 2).

Participants provided covariate information on their Facebook friends and gender. We included actors with this information who participated in at least one durational event in both communication modes (physical and digital), ensuring identifiable popularity coefficients. This amounts to 155,316 physical and 4,152 digital interactions among $N = 400$ actors. In Section B.6, we use instantaneous text messages from the participants to show the algorithm’s applicability to event data without duration.

5.1 Model Specification

To examine endogenous effects, we use summary statistics from Section 2.2. We evaluate whether actors i and j currently share and have previously shared a common partner, and we account for pairwise past interactions. For call events, having a common partner at the time of the event is impossible, as an individual can participate in only one phone call at a time. Accordingly, we exclude the current common partner terms from the corresponding incidence and duration models. We incorporate covariates related to Facebook friendships ($\mathbf{z}_1 = (z_{i,j,1})$, where $x_{i,j,1} = 1$ if actors i and j are Facebook friends) and gender ($\mathbf{x}_2 = (x_{i,2})$,

where $x_{i,2} = 1$ if actor i is female) as dyadic and monadic statistics, respectively: $z_{i,j,1} = x_{i,j,1}$ for dyadic relationships and $z_{i,j,2} = \mathbb{I}(x_{i,2} = x_{j,2})$ for gender homophily.

Substantial heterogeneity in interaction frequency across actors for both physical and digital events (see Section B.3), motivates the inclusion of actor-specific popularity parameters in the model. Interaction frequencies are expected to fluctuate considerably throughout the day since students are more likely to interact during the daytime hours. Thus, we let the baseline function $f(t, \gamma)$ change hourly, implying $Q = 672$. We conduct a sensitivity analysis in Section B.5 showing that letting $f(t, \gamma)$ to change every two hours does not substantially affect the results. While solving this problem is infeasible with state-of-the-art techniques, our novel algorithm enables model estimation in less than five minutes on a standard laptop.

5.2 Results

The parameter estimates $\hat{\alpha}$ reveal distinct patterns governing the incidence and duration of physical and digital interaction events. We provide the popularity and temporal estimates in Section B.3.

In the incidence model, shared current common partners are a key determinant of physical interactions. The first shared partner between actors i and j increases the corresponding event intensity by a multiplicative factor of 7.295. This coefficient confirms that joining an existing group of people is much more likely than starting a physical interaction with a single actor. General common partners also affect the event intensities. However, their effects are moderate: they increase the incidence intensity of physical interactions by a multiplicative factor of 1.654 and of digital interactions by 1.168 in the same setting. Besides these triadic closure effects, repeated interactions affect the incidence intensity. The first interaction between arbitrary actors i and j increases $\lambda_{i,j}^{0 \rightarrow 1}(t \mid \mathcal{H}_t, \theta^{0 \rightarrow 1})$ of physical

Table 2: Parameter estimates ($\hat{\alpha}$) and corresponding standard errors (SE) of the Durational Event Model applied to physical (co-location, columns 2-4) and digital (call, columns 5-7) interaction data. The column $2^{\hat{\alpha}}$ shown for statistics transformed by $\log(\cdot + 1)$ represents the effect of the first change in the respective statistic.

Statistic	Physical (Co-location)			Digital (Call)		
	$\hat{\alpha}$	SE	$2^{\hat{\alpha}}$	$\hat{\alpha}$	SE	$2^{\hat{\alpha}}$
Incidence ($\hat{\alpha}^{0 \rightarrow 1}$)						
Current Common Partner	2.867	.006	7.295			
General Common Partner	.726	.007	1.654	.224	.125	1.168
Number Interaction	1.129	.005	2.187	1.631	.039	3.097
Friendship Match	.383	.010		5.687	.116	
Both Female	-.021	.010		.203	.085	
Duration ($\hat{\alpha}^{1 \rightarrow 0}$)						
Number Interaction	-.158	.005	.896	-.274	.073	.827
Current Interaction	-.102	.002	.932	-.053	.024	.964
Current Common Partner	-.312	.006	.806			
General Common Partner	.080	.009	1.057	.518	.186	1.432
Friendship Match	-.535	.010		-.337	.464	
Both Female	-.018	.010		-.227	.320	

and digital interactions by multiplicative factors of 2.187 and 3.097, respectively. By the interpretation shown in (4), a shared Facebook friend affects the incidence intensity of digital communication by the multiplicative factor $\exp(5.687) \approx 295$. The incidence intensity of physical meetings is increased only by the factor $\exp(.383) \approx 1.46$ in the same setting. We estimate divergent effects for gender homophily. The incidence intensity of digital interaction between two female actors is significantly higher than for pairs where both actors are not

female. However, for physical interactions, we observe the opposite effect.

Both the number of current common partners and prior interactions significantly prolong physical interactions. The first current common partner and interaction reduce the duration intensity by multiplicative factors of 0.806 and 0.896, respectively. Similarly, shared friendship status approximately halves the duration intensity of physical interactions. This finding suggests that strong relational ties stabilize over time. In contrast, gender homophily does not have a statistically significant effect on the duration intensity of physical interactions. The durations of digital interactions, measured via call events, are driven by similar factors. However, in this case, all exogenous effects do not significantly differ from zero.

5.3 Model Assessment

To ensure that the estimated model adequately fits the observed data, we assess in-sample fit via Cox-Snell residuals and out-of-sample prediction. The time rescaling theorem (Brown et al., 2002) establishes for a correctly specified model that integrating all conditional intensities over their respective piecewise constant intervals yields a sequence of independent and identically distributed unit exponential random variables. These quantities, termed Cox-Snell residuals, are right-censored for the final interval of each dyad. Therefore, we evaluate goodness-of-fit by comparing a nonparametric Kaplan-Meier estimator of the survival function, defined as $\mathbb{P}(X > t)$ with $t > 0$ for a nonnegative random variable X , against the corresponding theoretical value, where $\mathbb{P}(X > t) = \exp(-t)$ holds under $X \sim \text{Exp}(1)$. As illustrated in Figure 3 (a), the estimated survival functions for both physical (black) and digital (blue) interactions closely follow the theoretical curve, suggesting that the proposed model accurately recovers the temporal structure of the data.

Following Vu et al. (2011), we assess out-of-sample fit by holding out the chronologically last 20% of events in the model for physical and digital interaction. With the remaining

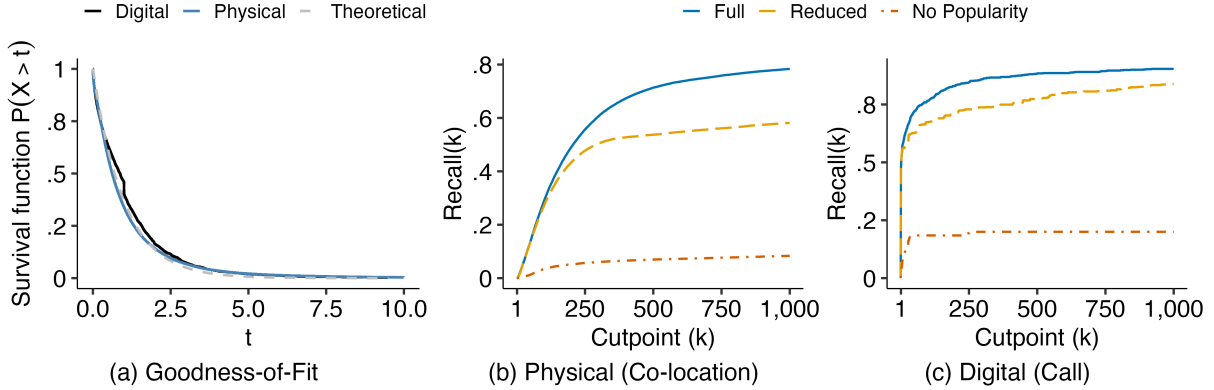


Figure 3: (a) Comparison of empirical and theoretical survival functions. (b) and (c): Top- k recall curves applied to physical (b) and digital (c) interaction data for three model specifications: Full (blue), Reduced (yellow), and No Popularity Models (orange).

80% of the data, we re-estimate three model specifications: the full model in Section 5.1 (Full), a reduced model with only friendship and gender statistics (Reduced), and the full model without popularity terms (No Popularity). With (3), the probability of an event between actors i and j to be the first after time t is given for any specification by:

$$\mathbb{P}((i, j) \text{ is next event after } t) = \frac{\lambda_{i,j}(t \mid \mathcal{H}_t, \boldsymbol{\theta})}{\sum_{(h,k) \in \mathcal{D}(t)} \lambda_{h,k}(t \mid \mathcal{H}_t, \boldsymbol{\theta})}. \quad (16)$$

For each event in the last 20% of events, we rank the top- k most likely events according to each of the three models and record whether the observed event falls within the respective top- k list. After each event, we update the sufficient statistics and iterate this procedure for the next event in the test set. The resulting top- k recall measure for $k \in \{1, \dots\}$ and a model is the fraction of events in the test set within the top- k predictions. As illustrated in Figure 3 (b) & (c), the full specification yields the best predictive power.

6 Conclusion

The proposed framework, accompanied by a scalable estimation algorithm and implementation in the DEM package, offers a foundation for modeling the dynamics of durational events. Nonetheless, there are still several avenues for extensions. For massive populations, it is reasonable to assume that durational events between actors i and j are primarily influenced by their respective local neighborhoods, rather than by the entire network. This assumption can be represented by local dependence (Schweinberger and Handcock, 2015), which can be extended to the context of durational events. Concerning algorithmic enhancements, it will be worthwhile to combine sample-based approximations (Raftery et al., 2012) or online algorithms (Corneck et al., 2025) with our coordinate ascent algorithm.

References

- Aalen, O. O. and Gjessing, H. K. (2007), Stochastic processes in survival analysis, *in* ‘Advances in Statistical Modeling and Inference’, pp. 23–43.
- Brown, E. N., Barbieri, R., Ventura, V., Kass, R. E. and Frank, L. M. (2002), ‘The Time-Rescaling Theorem and Its Application to Neural Spike Train Data Analysis’, *Neural Computation* **14**(2), 325–346.
- Butts, C. T. (2008), ‘A relational event framework for social action’, *Sociological Methodology* **38**(1), 155–200.
- Corneck, J., Cohen, E. A. K., Martin, J. S. and Passino, F. S. (2025), ‘Online Bayesian changepoint detection for network Poisson processes with community structure’, *Statistics and Computing* **35**(3), 75.
- Eagle, N. and Pentland, A. (2006), ‘Reality mining: Sensing complex social systems’, *Personal and Ubiquitous Computing* **10**(4), 255–268.

- Fritz, C., Mehrl, M., Thurner, P. W. and Kauermann, G. (2023), ‘All that glitters is not gold: Relational events models with spurious events’, *Network Science* **11**(2), 184–204.
- Granovetter, M. (1973), ‘The strength of weak ties’, *American Journal of Sociology* **78**(6), 1360–1380.
- Hoffman, M., Block, P., Elmer, T. and Stadtfeld, C. (2020), ‘A model for the dynamics of face-to-face interactions in social groups’, *Network Science* **8**(S1), 1–22.
- Hummel, R. M., Hunter, D. R. and Handcock, M. S. (2012), ‘Improving simulation-based algorithms for fitting ERGMs’, *Journal of Computational and Graphical Statistics* **21**, 920–939.
- Hunter, D. R. (2007), ‘Curved exponential family models for social networks’, *Social Networks* **29**(2), 216–230.
- Kitts, J. A., Lomi, A., Mascia, D., Pallotti, F. and Quintane, E. (2017), ‘Investigating the Temporal Dynamics of Interorganizational Exchange: Patient Transfers among Italian Hospitals’, *American Journal of Sociology* **123**(3), 850–910.
- Kreiß, A., Mammen, E. and Polonik, W. (2019), ‘Nonparametric inference for continuous-time event counting and link-based dynamic network models’, *Electronic Journal of Statistics* **13**(2), 2764–2829.
- Krivitsky, P. N. and Handcock, M. S. (2014), ‘A separable model for dynamic networks’, *Journal of the Royal Statistical Society: Series B (Statistical Methodology)* **76**(1), 29–46.
- Lange, K., Hunter, D. R. and Yang, I. (2000), ‘Optimization transfer using surrogate objective functions’, *Journal of Computational and Graphical Statistics* **9**, 1–20.
- Lazer, D., Pentland, A., Adamic, L., Aral, S., Barabási, A. L., Brewer, D., Christakis, N.,

- Contractor, N., Fowler, J., Gutmann, M., Jebara, T., King, G., Macy, M., Roy, D. and Van Alstyne, M. (2009), ‘Computational social science’, *Science* **323**(5915), 721–723.
- Lerner, J., Bussmann, M., Snijders, T. A. B. and Brandes, U. (2013), ‘Modeling frequency and type of interaction in event networks’, *Corvinus Journal of Sociology and Social Policy* **4**(1), 3–32.
- Lerner, J. and Lomi, A. (2020), ‘Reliability of relational event model estimates under sampling: How to fit a relational event model to 360 million dyadic events’, *Network Science* **8**(1), 97–135.
- Matias, C., Rebafka, T. and Villers, F. (2018), ‘A semiparametric extension of the stochastic block model for longitudinal networks’, *Biometrika* **105**(3), 665–680.
- Murphy, S. A. and van der Vaart, A. W. (2000), ‘On Profile Likelihood’, *Journal of the American Statistical Association* **95**(450), 449–465.
- Passino, F. S. and Heard, N. A. (2023), ‘Mutually Exciting Point Process Graphs for Modeling Dynamic Networks’, *Journal of Computational and Graphical Statistics* **32**(1), 116–130.
- Portnoy, S. (1988), ‘Asymptotic behavior of likelihood methods for exponential families when the number of parameters tends to infinity’, *The Annals of Statistics* **16**(1), 356–366.
- Raftery, A. E., Niu, X., Hoff, P. D. and Yeung, K. Y. (2012), ‘Fast inference for the latent space network model using a case-control approximate likelihood’, *Journal of Computational and Graphical Statistics* **21**, 901–919.
- Rastelli, R. and Fop, M. (2020), ‘A stochastic block model for interaction lengths’, *Advances in Data Analysis and Classification* **14**(2), 485–512.
- Sapiezynski, P., Stopczynski, A., Lassen, D. D. and Lehmann, S. (2019), ‘Interaction data from the Copenhagen Networks Study’, *Scientific Data* **6**(1), 315.

- Schweinberger, M. and Handcock, M. S. (2015), ‘Local dependence in random graph models: Characterization, properties and statistical inference’, *Journal of the Royal Statistical Society. Series B (Statistical Methodology)* **77**(3), 647–676.
- Sekara, V., Stopczynski, A. and Lehmann, S. (2016), ‘Fundamental structures of dynamic social networks’, *Proceedings of the National Academy of Sciences* **113**(36), 9977–9982.
- Snijders, T. A. B. and Van Duijn, M. A. J. (1997), Simulation for statistical inference in dynamic network models, *in* R. Conte, R. Hegselmann and P. Terna, eds, ‘Simulating Social Phenomena’, Springer-Verlag, Berlin, pp. 493–512.
- Stadtfeld, C., Hollway, J. and Block, P. (2017), ‘Dynamic network actor models: Investigating coordination ties through time’, *Sociological Methodology* **47**(1), 1–40.
- Stopczynski, A., Sekara, V., Sapiezynski, P., Cuttone, A., Madsen, M. M., Larsen, J. E. and Lehmann, S. (2014), ‘Measuring Large-Scale Social Networks with High Resolution’, *PLOS ONE* **9**(4), e95978.
- Ureña-Carrion, J., Saramäki, J. and Kivelä, M. (2020), ‘Estimating tie strength in social networks using temporal communication data’, *EPJ Data Science* **9**(1), 1–20.
- Vu, D. Q., Asuncion, A. U., Hunter, D. R. and Smyth, P. (2011), ‘Continuous-time regression models for longitudinal networks’, *NeurIPS* pp. 2492–2500.
- Vu, D. Q., Hunter, D. R. and Schweinberger, M. (2013), ‘Model-based clustering of large networks’, *The Annals of Applied Statistics* **7**(2), 1010–1039.
- Wagner, C., Strohmaier, M., Olteanu, A., Kıcıman, E., Contractor, N. and Eliassi-Rad, T. (2021), ‘Measuring algorithmically infused societies’, *Nature* **595**(7866), 197–204.

Supplementary material

Scalable Durational Event Models: Application to Physical and Digital Interactions

Cornelius Fritz^{1*}, Riccardo Rastelli^{2†}, Michael Fop^{2†}, Alberto Caimo^{2†}

¹School of Computer Science and Statistics, Trinity College Dublin

²School of Mathematics and Statistics, University College Dublin

A	Further Information on the Simulation Study	3
	A.1 Simulation of Durational Events	3
	A.2 Definition of Performance Measures	5
	A.3 Further Results	6
	A.3.1 Simulation Study 1	6
	A.3.2 Simulation Study 4: Computational Complexity with M	7
	A.3.3 Simulation Study 5: Choice of Q	8
B	Further Information on the Application	10
	B.1 Initial Censoring	10
	B.2 Descriptive Plots	11
	B.3 Popularity and Baseline Estimates	11

***Corresponding author:** fritzc@tcd.ie.

†Riccardo Rastelli, Michael Fop, and Alberto Caimo contributed equally to the work. Alberto Caimo conceived the original idea of the model.

B.4	Model Assessment	14
B.5	Sensitivity Analysis of Change-Point Specification	15
B.6	REM Application to Texting	17

A Further Information on the Simulation Study

A.1 Simulation of Durational Events

We can reformulate our data representation in an equivalent form, as follows: a durational event is characterized by two tuples in the form (i, j, t, r) , where t is a time stamp, and r is a binary indicator that determines if the tuple refers to the beginning ($r = 1$) or end ($r = 0$) of an interaction. Then we can equivalently represent durational event $d = (i, j, t_b, t_e)$ by $d_{\text{start}} = (i, j, t_b, 1)$ and $d_{\text{end}} = (i, j, t_e, 0)$. This is the format used for the provided R package DEM and in the following description of the pseudo-code to sample durational events from 2.

We present algorithm 1 for sampling durational events within an arbitrary time frame $(0, T]$ under the assumption that $f(t, \gamma^{0 \rightarrow 1})$ and $f(t, \gamma^{1 \rightarrow 0})$ remain constant in that interval. When these baseline step functions vary over time as step functions, we apply Algorithm 1 separately to each interval and concatenate the results. To accommodate for a flexible specification of $\mathcal{D}^{0 \rightarrow 1}(t)$ and $\mathcal{D}^{1 \rightarrow 0}(t)$, we include for each pair $(i, j) \in \mathcal{D}$ an indicator $p_{i,j}(t) \in \{0, 1\}$ of whether any type of event, start or end, is possible between the actors at time $t \in \mathcal{T}$. Our algorithm, therefore, assumes the specification of the following terms:

1. Number of actors N in the durational event network.
2. Sets of summary statistics for the incidence and duration model, $\mathbf{s}_{i,j}^{0 \rightarrow 1}(\mathcal{H}_t)$ and $\mathbf{s}_{i,j}^{1 \rightarrow 0}(\mathcal{H}_t)$.
3. Parameter vectors $\boldsymbol{\alpha}^{0 \rightarrow 1}$ and $\boldsymbol{\alpha}^{1 \rightarrow 0}$ for the summary statistics.
4. Parameter vectors $\boldsymbol{\beta}^{0 \rightarrow 1} \in \mathbb{R}^N$ and $\boldsymbol{\alpha}^{1 \rightarrow 0}$ for the popularity effects.
5. Parameters $f(0, \gamma^{0 \rightarrow 1})$ and $f(0, \gamma^{1 \rightarrow 0})$.

Together, these parameters are defining $\boldsymbol{\theta}^{0 \rightarrow 1}$ and $\boldsymbol{\theta}^{1 \rightarrow 0}$. Denoting all durational events

Result: Durational Event Matrix $E \in \mathbb{R}^{L \times 4}$, $E_{i,1}, E_{i,2} \in \mathcal{A}$, $E_{i,3} \in \mathcal{T}$,
 $E_{i,4} \in \{0, 1\}$ for $i \in \mathcal{A}$, where L is the maximal number of events.

Set $t_{\text{curr}} = 0$ and $n_{\text{ev}} = 0$. **while** $t_{\text{curr}} < T$ *or* $n_{\text{ev}} < L$ **do**

1. Step: Compute Intensities

Set

$$\lambda_{i,j}^{0 \rightarrow 1}(t_{\text{curr}} \mid \mathcal{H}_{t_{\text{curr}}}, \boldsymbol{\theta}^{0 \rightarrow 1}) = \exp\left(\boldsymbol{\alpha}^{0 \rightarrow 1} \mathbf{s}_{i,j}^{0 \rightarrow 1}(\mathcal{H}_{t_{\text{curr}}}) + \beta_i^{0 \rightarrow 1} + \beta_j^{0 \rightarrow 1} + f(0, \gamma^{0 \rightarrow 1})\right)$$

and

$$\lambda_{i,j}^{1 \rightarrow 0}(t_{\text{curr}} \mid \mathcal{H}_{t_{\text{curr}}}, \boldsymbol{\theta}^{1 \rightarrow 0}) = \exp\left(\boldsymbol{\alpha}^{1 \rightarrow 0} \mathbf{s}_{i,j}^{1 \rightarrow 0}(\mathcal{H}_{t_{\text{curr}}}) + \beta_i^{1 \rightarrow 0} + \beta_j^{1 \rightarrow 0} + f(0, \gamma^{1 \rightarrow 0})\right)$$

for all $(i, j) \in \mathcal{D}$.

2. Step: Select Intensities

Set $\boldsymbol{\lambda}(t_{\text{curr}} \mid \mathcal{H}_{t_{\text{curr}}}, \boldsymbol{\theta}^{0 \rightarrow 1}, \boldsymbol{\theta}^{1 \rightarrow 0}) = (\lambda_{i,j}(t_{\text{curr}} \mid \mathcal{H}_{t_{\text{curr}}}, \boldsymbol{\theta}^{0 \rightarrow 1}, \boldsymbol{\theta}^{1 \rightarrow 0}))$

$$\begin{aligned} \lambda_{i,j}(t_{\text{curr}} \mid \mathcal{H}_{t_{\text{curr}}}, \boldsymbol{\theta}^{0 \rightarrow 1}, \boldsymbol{\theta}^{1 \rightarrow 0}) &= ((1 - f_{i,j}(t_{\text{curr}})) \lambda_{i,j}^{0 \rightarrow 1}(t_{\text{curr}} \mid \mathcal{H}_{t_{\text{curr}}}, \boldsymbol{\theta}^{0 \rightarrow 1}) \\ &\quad + f_{i,j}(t_{\text{curr}}) \lambda_{i,j}^{1 \rightarrow 0}(t_{\text{curr}} \mid \mathcal{H}_{t_{\text{curr}}}, \boldsymbol{\theta}^{1 \rightarrow 0})) p_{i,j}(t) \end{aligned}$$

for all $(i, j) \in \mathcal{D}$.

3. Step: Sample Time Increment

Sample time between successive events:

$$T^* \sim \text{Exp}(\|\boldsymbol{\lambda}(t_{\text{curr}} \mid \mathcal{H}_{t_{\text{curr}}}, \boldsymbol{\theta}^{0 \rightarrow 1}, \boldsymbol{\theta}^{1 \rightarrow 0})\|_0)$$

with observation t^* .

4. Step: Sample Event

Sample which pair will experience the event:

$$(I^*, J^*) \sim \text{Multinomial}\left(\frac{\boldsymbol{\lambda}(t_{\text{curr}} \mid \mathcal{H}_{t_{\text{curr}}}, \boldsymbol{\theta}^{0 \rightarrow 1}, \boldsymbol{\theta}^{1 \rightarrow 0})}{\|\boldsymbol{\lambda}(t_{\text{curr}} \mid \mathcal{H}_{t_{\text{curr}}}, \boldsymbol{\theta}^{0 \rightarrow 1}, \boldsymbol{\theta}^{1 \rightarrow 0})\|_0}, n = 1\right)$$

with observation (i^*, j^*) .

5. Step: Save Sampled Event

Set $E_{n_{\text{ev}},1} = i^*$, $E_{n_{\text{ev}},2} = j^*$, $E_{n_{\text{ev}},3} = t^* + t_{\text{curr}}$, and $E_{n_{\text{ev}},4} = 1 - f_{i^*,j^*}(t_{\text{curr}})$.

6. Step: Update History and Counters

Update $\mathbf{s}_{i,j}^{0 \rightarrow 1}(\mathcal{H}_{t+t_{\text{curr}}})$ and $\mathbf{s}_{i,j}^{1 \rightarrow 0}(\mathcal{H}_{t+t_{\text{curr}}})$ for all $(i, j) \in \mathcal{D}$.

Set $f_{i^*,j^*}(t_{\text{curr}} + t^*) = 1 - f_{i^*,j^*}(t_{\text{curr}})$, $t_{\text{curr}} = t^* + t_{\text{curr}}$, and $n_{\text{ev}} = n_{\text{ev}} + 1$.

end

Return $E[, 0 : (n_{\text{ev}} - 1)]$

Algorithm 1: Pseudo-Code to sample durational events in $(0, T]$.

that start before t by $\mathcal{D}(t)$, we can define the indicator function $f_{i,j}(t)$ whether actor pair $(i, j) \in \mathcal{D}$ are at time $t \in \mathcal{T}$ are in an ongoing duration

$$f_{i,j}(t) := \mathbb{I}(\exists d = (i, j, b, e) \in \mathcal{D}(t) \text{ such that } t \in [b, e]).$$

A.2 Definition of Performance Measures

The AVE of a specific estimate $\hat{\boldsymbol{\theta}}$ is the empirical mean of the estimates over the S datasets:

$$\text{AVE}(\hat{\boldsymbol{\theta}}) = \frac{1}{S} \sum_{s=1}^S \hat{\boldsymbol{\theta}}_{(s)},$$

where $\hat{\boldsymbol{\theta}}_{(s)} = (\hat{\alpha}_{(s)}, \hat{\beta}_{(s)}, \hat{\gamma}_{(s)})$ is the estimate of $\boldsymbol{\theta}$ in the s th simulation run. Given that all datasets are generated under the same parameter values, this statistic provides a meaningful assessment of estimation bias via

$$\text{bias}(\hat{\boldsymbol{\theta}}) = \text{AVE}(\hat{\boldsymbol{\theta}}) - \boldsymbol{\theta}^*,$$

where $\boldsymbol{\theta}^*$ is the data-generating parameter. To gauge both bias and variance, we report the RMSE of $\boldsymbol{\theta}$:

$$\text{RMSE}(\hat{\boldsymbol{\theta}}) = \sqrt{\frac{1}{S} \sum_{s=1}^S (\hat{\boldsymbol{\theta}}_{(s)} - \boldsymbol{\theta})^\top (\hat{\boldsymbol{\theta}}_{(s)} - \boldsymbol{\theta})}.$$

To assess uncertainty quantification when estimating $\boldsymbol{\alpha}$, we examine coverage probabilities. The coverage probability is the percentage of simulations in which the true parameter falls within the confidence interval based on the normal approximation:

$$Z_{(s)} = (-\Lambda(\hat{\boldsymbol{\theta}}_{(s)}))^{1/2}(\hat{\alpha}_{(s)} - \alpha^*) \sim \mathcal{N}(0, 1),$$

where $\Lambda(\hat{\boldsymbol{\theta}})$ is defined in (15) of the main article and refers to the block of the inverse Hessian corresponding to $\boldsymbol{\alpha}$. To validate this normal approximation, we compare the observed quantiles of $Z_{(s)}$ to those we expect from standard normal random variables.

A.3 Further Results

A.3.1 Simulation Study 1

In addition to assessing the coverage probability and accuracy of the parameter estimates demonstrated in Simulation Study 1 in the main manuscript, we assessed the effectiveness of model selection via the AIC and looked at Quantile-Quantile plots of the standardized estimates.

Model Selection The Akaike Information Criterion (AIC, Akaike, 1973) for the DEM with converged estimate $\hat{\theta} = (\hat{\theta}^{0 \rightarrow 1}, \hat{\theta}^{1 \rightarrow 0})$ under M events is given by the sum of the AIC of the incidence and duration model:

$$AIC^{0 \rightarrow 1} := 2p^{0 \rightarrow 1} - 2\ell(\hat{\theta}^{0 \rightarrow 1}) \text{ and } AIC^{1 \rightarrow 0} := 2p^{1 \rightarrow 0} - 2\ell(\hat{\theta}^{1 \rightarrow 0}), \quad (\text{A.1})$$

where $p^{0 \rightarrow 1}$ and $p^{1 \rightarrow 0}$ denote the total number of parameters in the incidence and duration model, respectively. We apply the following greedy model selection procedure: first, we fit a simple model where the incidence model only includes the current common partner, and the duration model has no covariates. Then, we calculate the AIC from (A.1) for this initial model. We proceed by adding covariates to the incidence structure in a step-wise fashion, one at a time. For each fitted model, we again calculate the AIC and retain the new model as optimal if a better criterion value is obtained. Once we converge to an optimal incidence model structure, we apply an analogous procedure to the duration model. The model achieving the highest value of the criterion, overall, is retained as the optimal inferred model. The inferred optimal model coincides with the data-generating model in all of the datasets generated in this experiment.

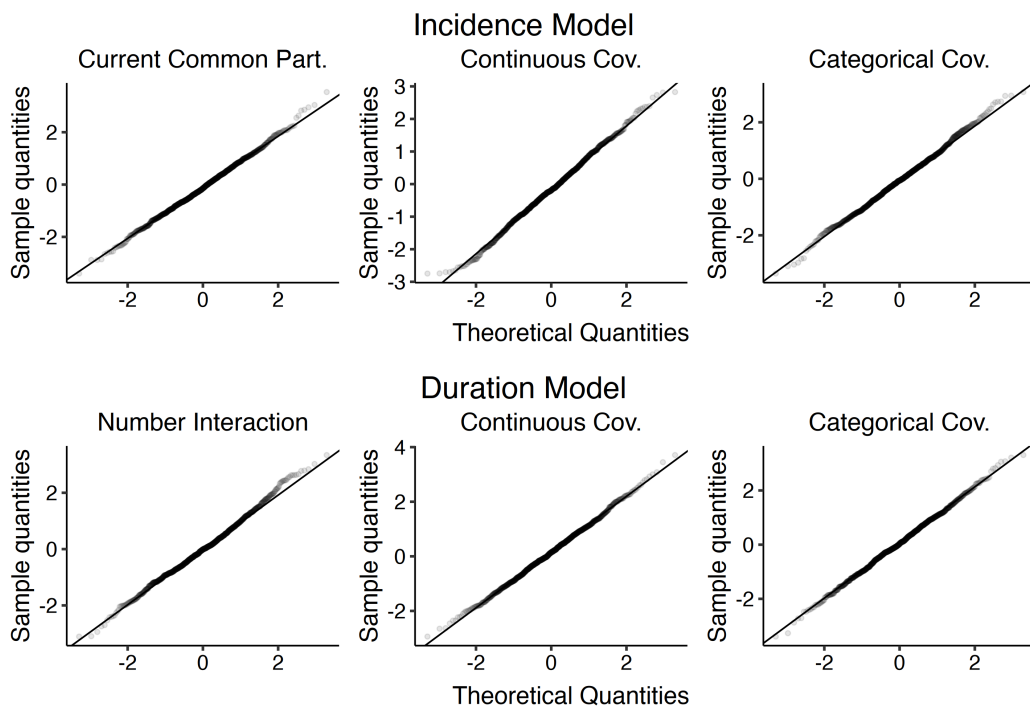


Figure 4: Simulation Study 1: Quantile-quantile plots for the incidence (top row) and duration model (bottom row) comparing the theoretical quantiles of a standard normal distribution with the sample quantiles of $z_{(s)} = \Lambda(\hat{\boldsymbol{\theta}}_{(s)})^{1/2}(\hat{\boldsymbol{\alpha}}_{(s)} - \boldsymbol{\alpha})$ for $s = 1, \dots, 1,000$.

Quantile-Quantile Plots of Standardized Estimates The quantile-quantile plots in Figure 4 illustrate a close alignment of sample quantiles with theoretical normal quantiles.

A.3.2 Simulation Study 4: Computational Complexity with M

Next, we investigate the performance of our estimator as M increases. Similar to Simulation Study 1, we fix $N = 500$. However, we set the baseline intensity to be a constant and sample an increasing number of events from this model. For each estimation run, we measure the execution time (in seconds) and peak memory allocation (in megabytes) for estimating the model.

Figure 5 shows a linear growth both in execution time and peak memory used in terms of

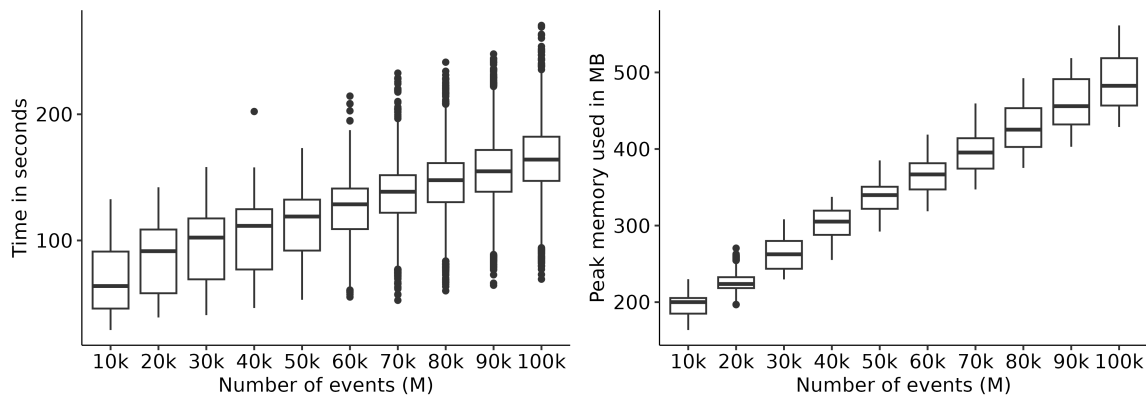


Figure 5: Simulation Study 4: Comparison of computational time (left) and memory needed for estimation (right) for different numbers of events (M) of our proposed three-step estimator.

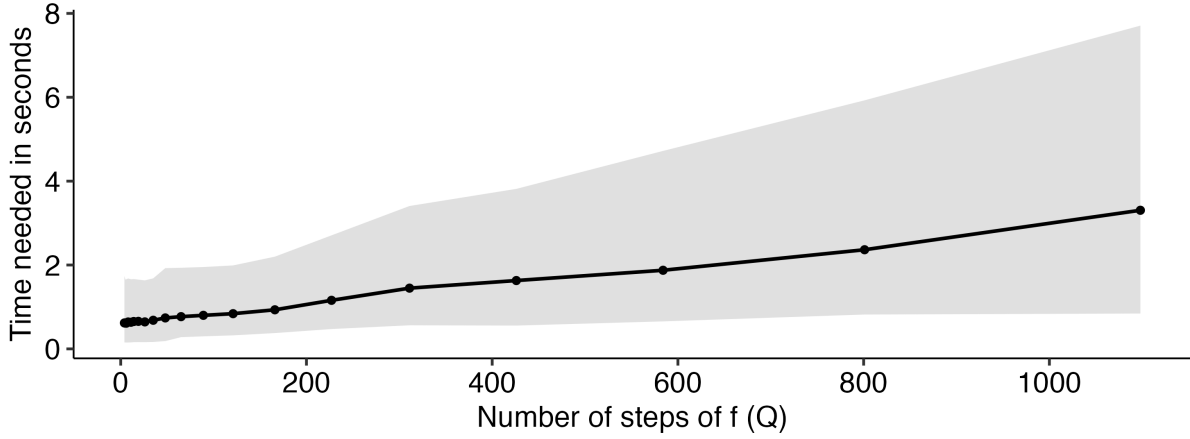
M . These results align with the provided complexity analysis from Section 3 and show how settings with larger M are not an issue for our algorithm.

A.3.3 Simulation Study 5: Choice of Q

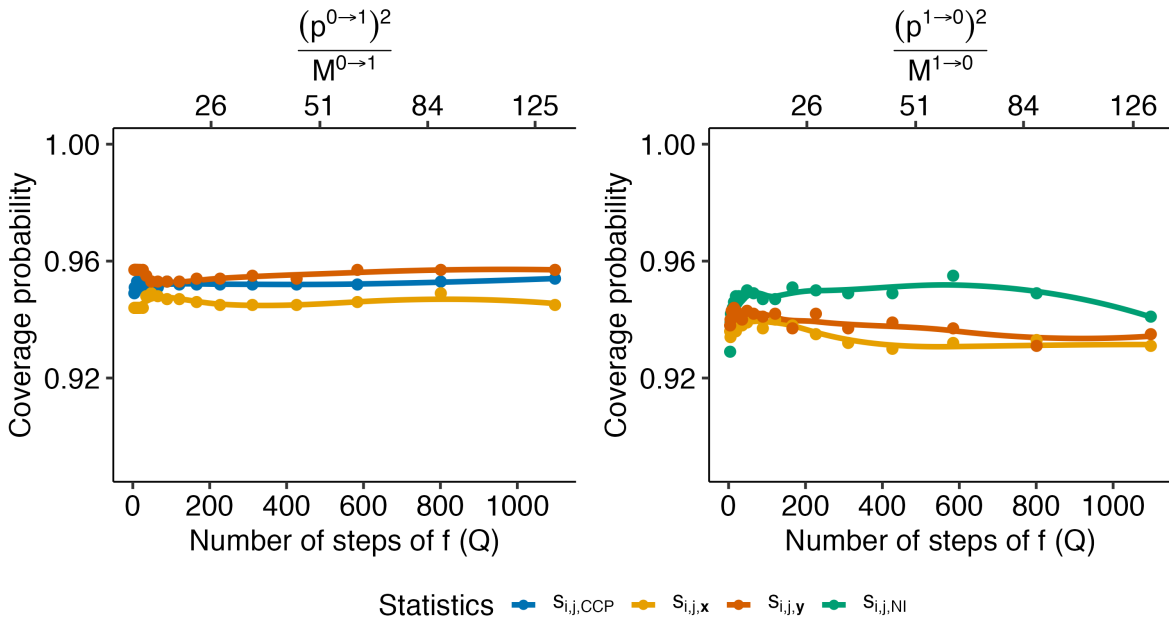
To estimate the DEM, one must choose the number of steps in the baseline intensity, $f(t, \gamma)$. Most times, we regard the parameters γ characterizing f as nuisance parameters when assessing the uncertainty of the parameters of interest, α . In Simulation Study 5, we assess two things:

1. The sensitivity of the coverage probabilities of α to mis-specifying Q .
2. The computational complexity with varying Q .

Using the same simulation setup as in Simulation Study 1 from Section 4, we re-estimate the model assuming baseline intensities and vary Q between 4 and 1098 in exponential steps, i.e., 4, 5, 6, ..., 584, 801, 1098. As with the other simulation studies, we repeat this simulation 1,000 times.



(a) Per-iteration update time for varying steps of $f(Q)$



(b) Coverage probability for varying steps of $f(Q)$

Figure 6: Simulation Study 5: Coverage probabilities of parameter of interest, α , under mis-specified Q . The dotted vertical line at $Q = 10$ represents the ground truth. The variables $p^{0 \rightarrow 1}$ and $p^{1 \rightarrow 0}$ denote the total number of parameters of the incidence and duration model, respectively, with corresponding number of starting and ending events given by $M^{0 \rightarrow 1}$ and $M^{1 \rightarrow 0}$.

In Figure 6 (a), we show that the linear growth of the computational complexity with respect to Q derived in Section 3 aligns with the empirical observed behavior. Figure 6

(b) illustrates that the coverage probabilities corresponding to all sufficient statistics are relatively constant around 95% with respect to the exact value of Q .

On the second upper x-axis of Figure 6 (b), we plot the squared number of estimated parameters over the number of events beginning (left) and ending (right) an interaction. The variables $p^{0 \rightarrow 1}$ and $p^{1 \rightarrow 0}$ thus denote the total number of parameters in the incidence and duration model, respectively. First, this provides evidence that the precise choice of Q does not affect the estimator’s accuracy or the uncertainty quantification. Second, the normal approximation still holds as the ratio of the squared number of parameters to the number of events diverges. These empirical results suggest that profiling out γ and making use of the theory of profile likelihoods still yields valid normal approximations as long as P and N do not grow faster than the square root of the respective number of events (Murphy and van der Vaart, 2000).

B Further Information on the Application

B.1 Initial Censoring

For our applications, we assume that the observations start with the first event. Chronologically ordering the observed events by d_1, \dots, d_M , we thus set $d_1 = (i_1, j_1, 0, e_1)$. We have no information on when exactly the observational process starts and, therefore, condition on the start of the first event without modeling it. While this approach overlooks the initial censoring of observations, the effect is negligible. This is a consequence of the fact that there are 155,316 and 4,152 proximity and call events, respectively, which outweigh the contribution of the first event.

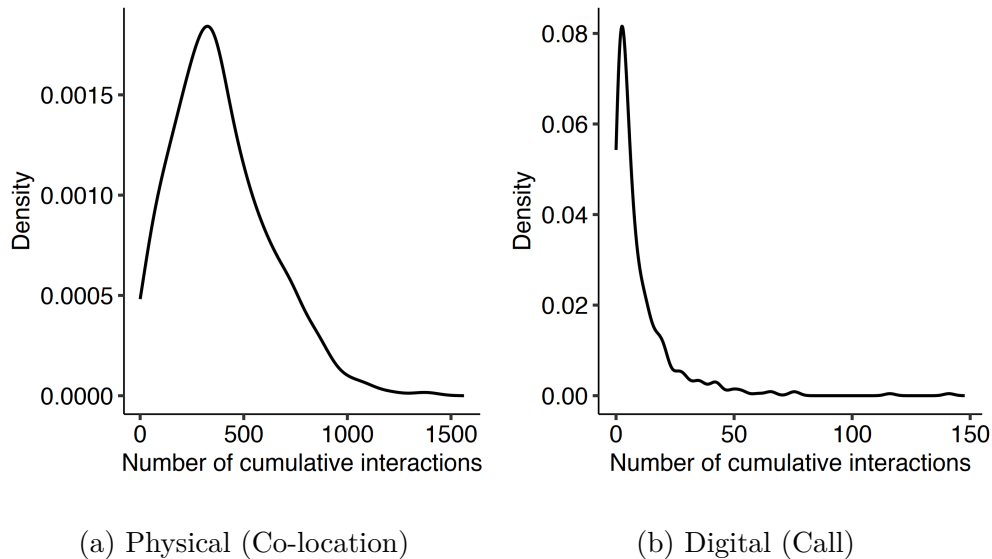


Figure 7: Application: Kernel-density estimator of cumulative durational events per actors for physical (a) and digital interactions (b).

B.2 Descriptive Plots

Figure 7 presents density estimators of the number of interactions individual actors are involved in for each event network. These distributions indicate substantial heterogeneity among actors in both settings and give rise to incorporating popularity coefficients.

B.3 Popularity and Baseline Estimates

Popularity Estimates. The number of potential actor pairs to begin interacting is typically orders of magnitude larger than the pairs that may end them, while the number of started and ended events is roughly the same. This imbalance is reflected in the overall level of estimates shown in Figure 8, where the average of $\hat{\beta}^{0 \rightarrow 1}$ is lower than the average of $\hat{\beta}^{1 \rightarrow 0}$ for both interaction modes. Consistent with Figure 7, the popularity parameters in the incidence model are generally higher for co-location than for call interactions. The contour lines in Figure 7 enable a comparison of individual actors' popularity estimates

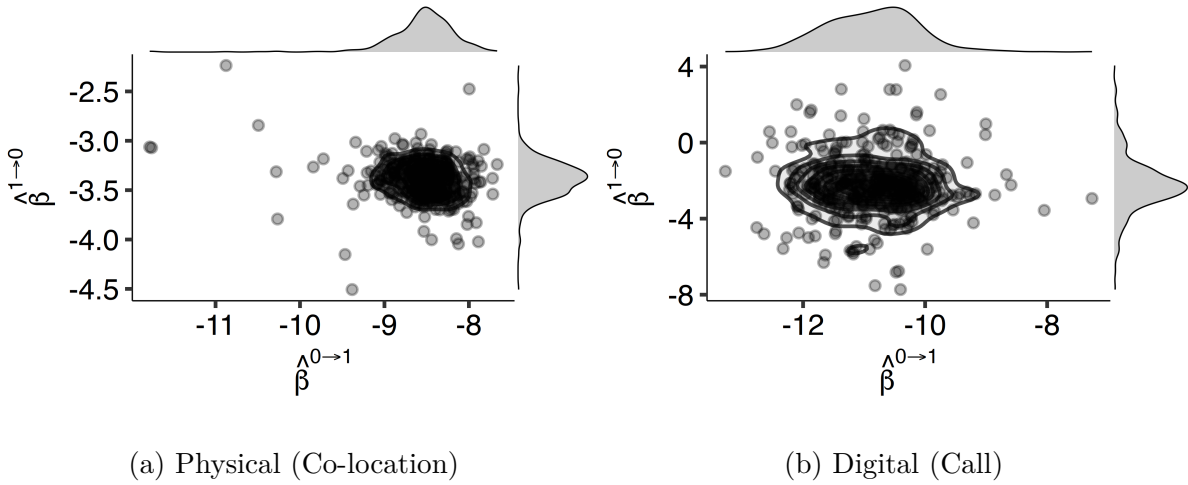


Figure 8: Estimates of the popularity parameters for physical (A) and digital interactions (B).

between the incidence and duration models. There is no clear correlation between the two estimates for physical interactions. However, a pattern emerges for digital interactions where low to average popularity coefficients in the incidence model often correspond to average popularity effects in the duration model.

Baseline Temporal Estimates. If no interaction is observed during a particular hour, we assume that the baseline did not change from the previous hour. Therefore, the number of parameters in γ fluctuates slightly between each estimated model.

The estimates of the baseline step functions $f(t, \hat{\gamma}^{0 \rightarrow 1})$ and $f(t, \hat{\gamma}^{1 \rightarrow 0})$ for the co-location and call data are presented in the first rows of Figures 9 and 10, respectively. As described in Section 5, each step in these step functions corresponds to a one-hour interval. A clear daily cyclical pattern is evident in Figures 9 and 10. To separate long-term trends from cyclical variations, we apply the local smoothing technique developed by Cleveland (1979) to each baseline step function independently. The resulting trend estimates are represented by black smooth lines in all plots.

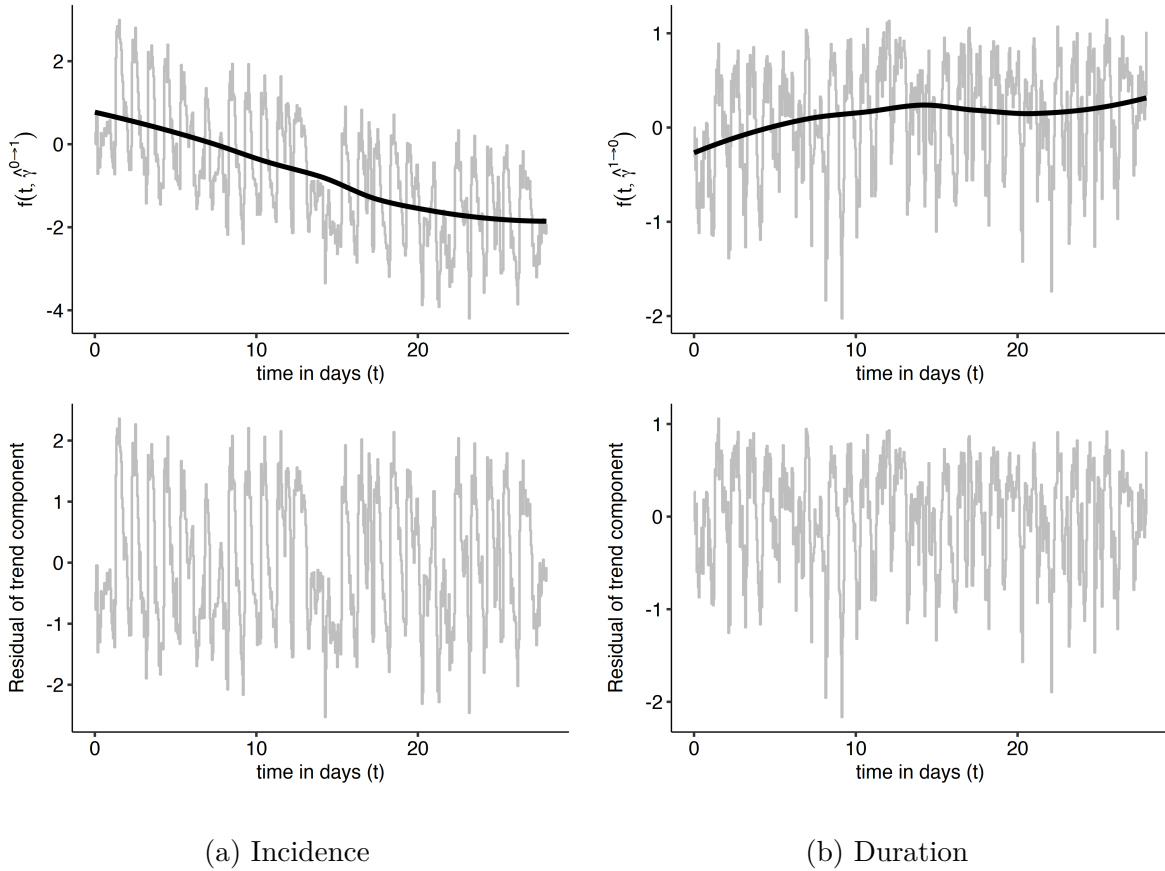


Figure 9: Estimates of baseline intensity of the co-location model.

From the first row of Figures 9 and 10, we observe that controlling for all other effects, the baseline step function for the initiation of a durational event shows a consistent decline over the observed period. In contrast, the baseline step function for terminating a durational event exhibits a slight increase or remains stable. The second row of these figures displays the residuals from the local regression, which capture cyclical effects. Notably, the step function residuals for the incidence models reveal strong daily patterns, where high intensities align with daylight hours and low intensities correspond to nighttime. Additionally, in the first plot of the second row in Figure 9, an apparent disruption in this pattern around day 15 may be associated with weekend activities.

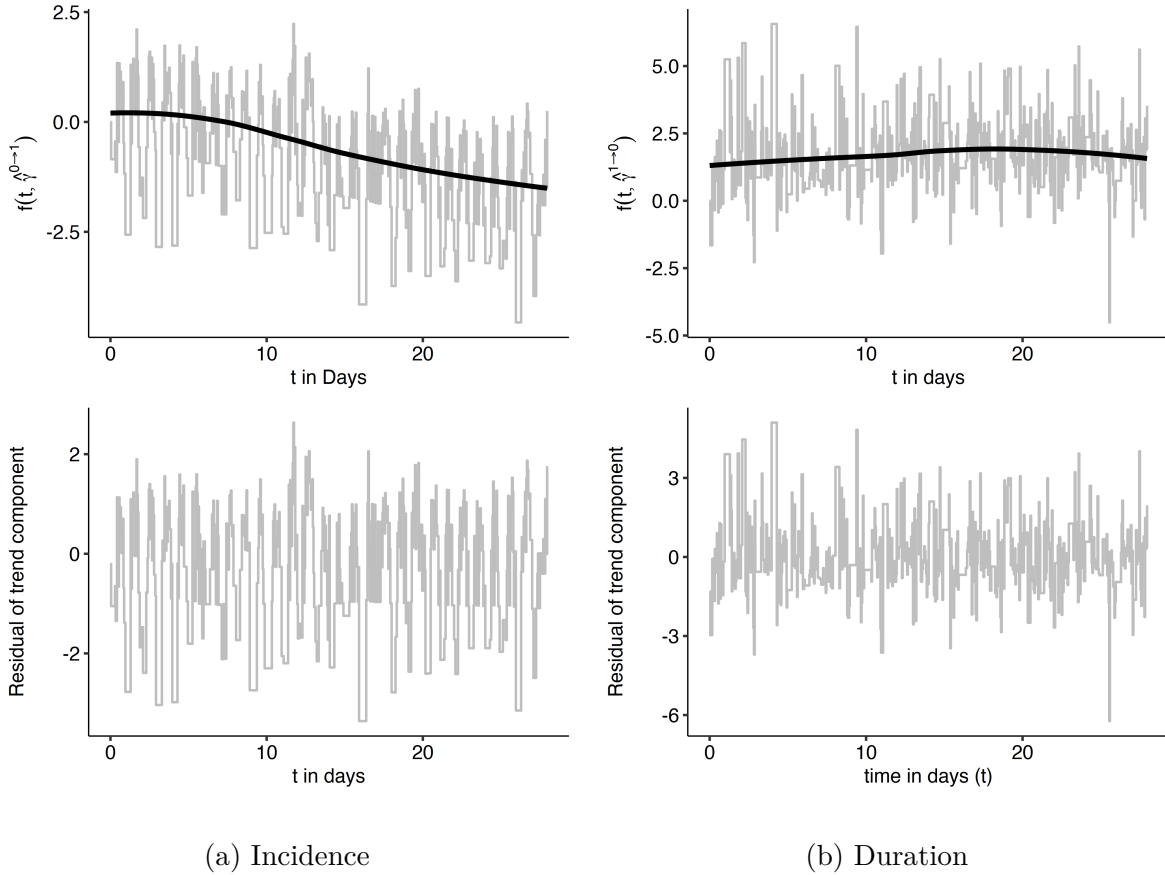


Figure 10: Estimates of baseline step function of the call model.

B.4 Model Assessment

Complementing the out-of-sample validation presented in the primary manuscript, Tables 3 and 4 provide parameter estimates derived from the subsample comprising the initial 80% of observed events. The results of the full model specification are consistent with those of the main manuscript, providing evidence that omitting 20% of the events does not affect the estimates much. Further, we report the AIC value for each specification in the final rows of Tables 3 and 4. Since lower values indicate better model fit, the results are consistent with the out-of-sample predictions reported in the main manuscript. Therefore, including popularity estimates and endogenous statistics improves model fit.

Table 3: Parameter estimates ($\hat{\alpha}$) and standard errors (SE) of the Durational Event Model applied to the co-location data.

	Full		Reduced		No Popularity	
	$\hat{\alpha}$	SE	$\hat{\alpha}$	SE	$\hat{\alpha}$	SE
Incidence ($\hat{\alpha}^{0 \rightarrow 1}$)						
Current Common Partner	2.730	.007			1.873	.008
General Common Partner	.638	.008			.085	.003
Number Interaction	1.153	.007			1.839	.005
Friendship Match	.504	.013	2.361	.013	-5.557	.009
Both Female	-.014	.012	.207	.012	-8.692	.011
Duration ($\hat{\alpha}^{1 \rightarrow 0}$)						
Current Interaction	-.073	.002			-.073	.002
Number Interaction	-.236	.007			-.236	.007
Current Common Partner	-.475	.008			-.475	.008
General Common Partner	.157	.011			.158	.011
Friendship Match	-.608	.013	-.730	.012	-.608	.013
Both Female	-.024	.013	-.046	.013	-.024	.013
AIC	4.068×10^5		5.34×10^5		1.9×10^8	

B.5 Sensitivity Analysis of Change-Point Specification

As detailed in the main text, the user must specify the set of change points $0 = c_0 < c_1 < \dots < c_Q$, at which the baseline step function $f(t, \gamma) = \sum_{q=1}^Q \gamma_q \mathbb{I}(c_{q-1} \leq t < c_q)$ is allowed to change. In the application presented in Section 5, we construct an hourly grid spanning the entire 27-day observation period. As a sensitivity check, we re-estimate the

Table 4: Parameter estimates ($\hat{\alpha}$) and standard errors (SE) of the Durational Event Model applied to the call data.

	Full		Reduced		No Popularity	
	$\hat{\alpha}$	SE	$\hat{\alpha}$	SE	$\hat{\alpha}$	SE
Incidence ($\hat{\alpha}^{0 \rightarrow 1}$)						
Number Interaction	1.642	.045			5.179	.026
General Common Partner	.143	.147			2.013	.154
Friendship Match	5.882	.134	7.436	.144	-8.195	.032
Both Female	.239	.091	.103	.075	-12.029	.060
Duration ($\hat{\alpha}^{1 \rightarrow 0}$)						
Current Interaction	-.025	.028			-.024	.028
Number Interaction	-.282	.082			-.303	.082
General Common Partner	.560	.216			.546	.217
Friendship Match	.570	.678	.506	.671	-.287	.640
Both Female	-.137	.338	-.015	.349	-.377	.338
AIC	2.195×10^4		2.466×10^4		1.892×10^8	

same models reported in Table 2, but under a coarser temporal resolution, allowing for a change point every two hours instead of one. The corresponding estimates of $\hat{\alpha}^{0 \rightarrow 1}$ and $\hat{\alpha}^{1 \rightarrow 0}$ under this specification are presented in Tables 5 and 6, while the estimated baseline step function $f(t, \hat{\gamma}^{0 \rightarrow 1})$ and $f(t, \hat{\gamma}^{1 \rightarrow 0})$ are visualized in Figure 11. All those results confirm the robustness of our results concerning the choice of grid resolution for change points. The estimated effects remain qualitatively the same, demonstrating that the model’s conclusions are not sensitive to the specific granularity of the baseline step function.

Table 5: Parameter estimates ($\hat{\alpha}$) and standard errors (SE) of the Durational Event Model applied to the co-location data assuming a baseline step function that can change every hour (left column) and every second hour(right column).

Summary Statistic	Every Hour		Every two hours	
	$\hat{\alpha}$	SE	$\hat{\alpha}$	SE
Incidence ($\hat{\alpha}^{0 \rightarrow 1}$)				
Current Common Partner	2.867	.006	2.834	.006
General Common Partner	.726	.007	.726	.007
Number Interaction	1.129	.005	1.127	.005
Friendship Match	.383	.010	.383	.010
Both Female	-.021	.010	-.020	.010
Duration ($\hat{\alpha}^{1 \rightarrow 0}$)				
Current Interaction	-.102	.002	-.101	.002
Number Interaction	-.158	.005	-.165	.005
Current Common Partner	-.312	.006	-.319	.006
General Common Partner	.080	.009	.086	.009
Friendship Match	-.535	.010	-.536	.010
Both Female	-.018	.010	-.017	.010

B.6 REM Application to Texting

For the application to the texting data between the students, we apply similar inclusion criteria as in the applications shown in the main analysis. However, we apply the condition that all included actors need to have at least one relational event, i.e., texting event. Thereby, we obtain 38,286 relational events between $N = 426$ students. Each relational

Table 6: Parameter estimates ($\hat{\alpha}$) and standard errors (SE) of the Durational Event Model applied to the call data assuming a baseline step function that can change every hour (left column) and every second hour(right column).

Summary Statistic	Every Hour		Every two hours	
	$\hat{\alpha}$	SE	$\hat{\alpha}$	SE
Incidence ($\hat{\alpha}^{0 \rightarrow 1}$)				
General Common Partner	1.631	.039	1.631	.039
Number Interaction	.224	.125	.227	.121
Friendship Match	5.687	.116	5.681	.116
Both Female	.203	.085	.201	.084
Duration ($\hat{\alpha}^{1 \rightarrow 0}$)				
Current Interaction	-.053	.024	-.060	.023
Number Interaction	-.274	.073	-.162	.065
General Common Partner	.518	.186	.579	.170
Friendship Match	-.337	.464	-.670	.390
Both Female	-.227	.320	-.211	.287

event $d = (i, j, t)$ is a tuple representing a text message between students i and j at time t .

In accordance with (2) , the intensity of an event at time $t \in \mathcal{T}$ for pair $(i, j) \in \mathcal{B}$ is:

$$\lambda_{i,j}(t | \mathcal{H}_t, \theta) = \exp\left(\alpha^\top \mathbf{s}_{i,j}(\mathcal{H}_t) + \beta_i + \beta_j + f(t, \gamma)\right). \quad (\text{B.1})$$

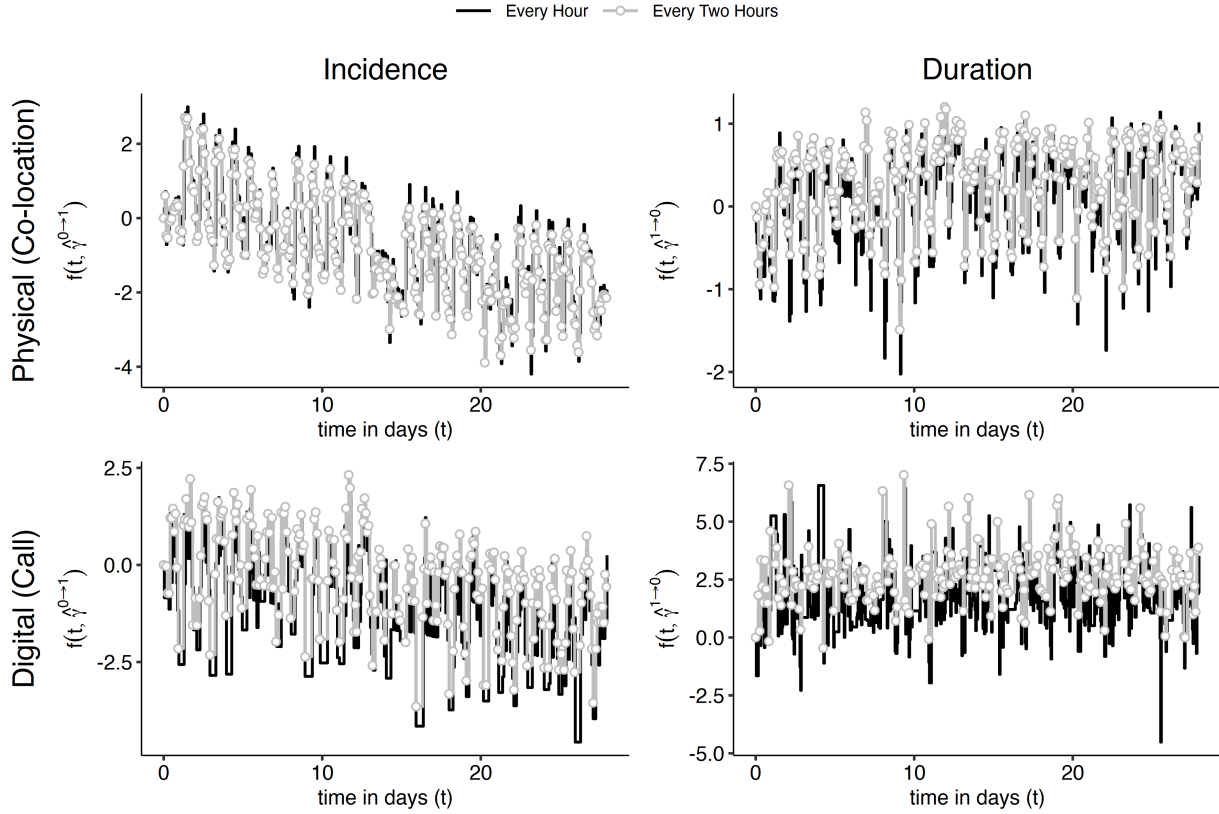


Figure 11: Comparison of the estimated baseline step function under the assumption that it can change every hour and every two hours for durational events representing co-location (first row) and call events (second row) for the incidence (first column) and duration model (second column).

The summary statistics are

$$\mathbf{s}_{i,j}(\mathcal{H}_t) = \begin{pmatrix} \log \left(\sum_{h \notin \{i,j\}} v_{i,h}(t) v_{h,j}(t) + 1 \right) \\ \log(N_{i,j}(t) + 1) \\ \mathbb{I}(x_{i,j,1} = 1) \\ \mathbb{I}(x_{i,2} = x_{j,2}) \end{pmatrix},$$

where $v_{i,j}(t)$ indicates whether actors i and j have ever interacted before time t . The covariates are defined in Section 5.

Table 7: Parameter estimates ($\hat{\alpha}$) and standard errors (SE) of the Relational Event Model applied to the Texting data.

Summary Statistic	$\hat{\alpha}$	SE	$2^{\hat{\alpha}}$
Common Partner	.321	.052	1.249
Number Interaction	2.226	.011	4.678
Friendship Match	-.419	.133	
Both Female	.229	.039	

Summary Statistics. The estimates of α are given in Table 7 and can be interpreted as detailed in Section 2.2. The first common partner and joint interaction have a multiplicative effect of 1.249 and 4.678 on the intensity between students i and j . These two coefficients demonstrate that sharing common text partner incentives triadic closure and that students repeatedly exchange texts between them. Contrary to these findings, being friends on Facebook has a small but significant negative effect on the intensity. Finally, we observe a positive gender-specific homophily effect, whereby two female students are more likely to exchange text messages than two males and mixed gender pairs.

Popularity Estimates. We visualize the observed dyadic text message exchanges in Figure 12 as a weighted network, where the weight of each edge represents the logarithm of the number of SMS events between the corresponding pair of students. We used the Fruchterman-Reingold algorithm (Fruchterman and Reingold, 1991) for this visualization. The size of each node is scaled relative to the corresponding popularity estimate $\hat{\beta}_i$. Figure 12 reveals that students with higher popularity estimates do not necessarily occupy central positions in the network. One possible explanation is that the interaction patterns between actors in central regions of the network are well captured by the summary statistics without

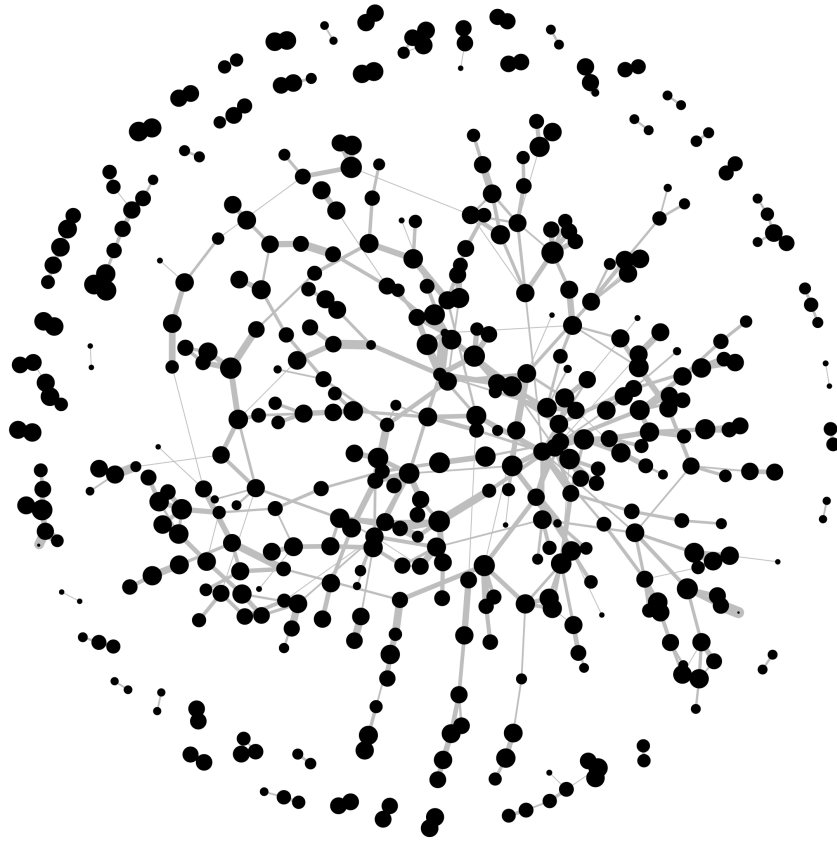


Figure 12: Observed texting events over the studied 28 days. The number of text messages between particular students is represented by the thickness of the edge and the size of the nodes represents the relative popularity estimate.

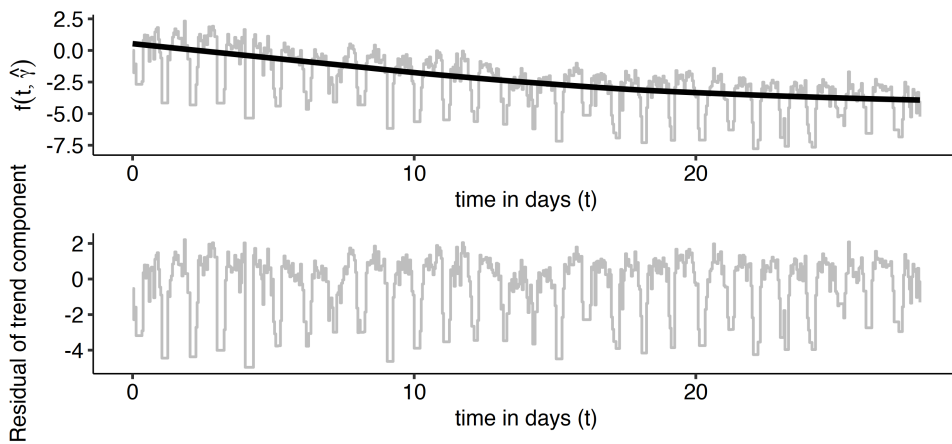


Figure 13: Estimated baseline step function for the REM applied to the Texting Data.

the need for additional popularity effects.

Baseline Step Function. Finally, we visualize the estimated baseline step function $f(t, \hat{\gamma})$ in Figure 13. Consistent with the patterns observed in Figures 9 and 10, the function exhibits distinct daily cycles alongside a gradual downward trend over time.

Supplementary Material References

Akaike, H. (1973). Information theory and an extension of the maximum likelihood principle.

Second International Symposium on Information Theory, 267–281.

Cleveland, W. S. (1979). Robust locally weighted regression and smoothing scatterplots.

Journal of the American Statistical Association 74(368), 829–836.

Fruchterman, T. M. J. and E. M. Reingold (1991). Graph drawing by force-directed

placement. *Software: Practice and Experience* 21(11), 1129–1164.